Article

Antagonistic circuits mediating infanticide and maternal care in female mice

https://doi.org/10.1038/s41586-023-06147-9

Received: 11 November 2021

Accepted: 27 April 2023

Published online: 7 June 2023

Check for updates

Long Mei[1]✉, Rongzhen Yan[1,5], Luping Yin[1,5], Regina M. Sullivan[2] & Dayu Lin[1,3,4]✉

In many species, including mice, female animals show markedly different pup-directed behaviours based on their reproductive state[1,2]. Naive wild female mice often kill pups, while lactating female mice are dedicated to pup caring[3,4]. The neural mechanisms that mediate infanticide and its switch to maternal behaviours during motherhood remain unclear. Here, on the basis of the hypothesis that maternal and infanticidal behaviours are supported by distinct and competing neural circuits[5,6], we use the medial preoptic area (MPOA), a key site for maternal behaviours[7–11], as a starting point and identify three MPOA-connected brain regions that drive differential negative pup-directed behaviours. Functional manipulation and in vivo recording reveal that oestrogen receptor α (ESR1)-expressing cells in the principal nucleus of the bed nucleus of stria terminalis (BNSTpr^{ESR1}) are necessary, sufficient and naturally activated during infanticide in female mice. MPOA^{ESR1} and BNSTpr^{ESR1} neurons form reciprocal inhibition to control the balance between positive and negative infant-directed behaviours. During motherhood, MPOA^{ESR1} and BNSTpr^{ESR1} cells change their excitability in opposite directions, supporting a marked switch of female behaviours towards the young.

At birth, young animals are vulnerable and powerless for nearly all mammalian species. Their chance of survival is critically dependent on care and protection from the parents, especially the mothers. Consequently, a set of robust and stereotypical maternal behaviours, such as nursing, crouching, grooming and retrieving, have evolved to ensure the needs of the young are met. However, female mammals do not always care for pups. Across a wide range of mammalian species, it is not uncommon for virgin female animals to show hostile behaviours towards pups of the same species[12,13]. In a survey involving 289 mammalian species, infanticide was found in 31% of species, with a higher percentage in species that breed in groups[12]. Despite the prevalence of infanticide in female mammals, including mice[3,4], it is rarely studied under laboratory conditions partly because adult female mice of many inbred strains, for example, C57BL/6, rarely show such behaviour, probably due to inbreeding[14,15]. Female mice of outbred strains, for example, Rockland-Swiss, appear to have retained more naturalistic behaviours, including a higher level of infanticide compared with inbred mice, although the exact likelihood varies with age[16].

The neural circuit of maternal behaviours has been extensively studied, and the medial preoptic area (MPOA) has been firmly established as a critical region for maternal behaviours[7–11]. Recent studies further revealed MPOA cells expressing ESR1 (MPOA^{ESR1})[17,18] or galanin[19,20] as the key populations facilitating maternal behaviours, such as pup retrieval and grooming. Notably, MPOA cells that are relevant for parental behaviours are mainly inhibitory[18,19,21]. In fact, activating GABAergic cells in the MPOA is sufficient to elicit pup retrieval and nest building[22], whereas activating MPOA glutamatergic cells elicits anxiety-like behaviours[23].

In contrast to our extensive knowledge of the maternal circuit, little is known regarding the neural substrates responsible for infanticide in female mice. A few recent studies revealed neural substrates that are relevant for infanticide in males. Lesioning rhomboid nucleus of the bed nucleus of stria terminalis[24] or inactivating urocortin-3 cells in perifornical area[25] reduced pup attack, whereas activating the amygdalohippocampal area[26] or GABAergic cells in the medial amygdala posterodorsal part (MeApd)[27] promoted pup attack in males. However, the roles of these regions in female infanticide are either minimal or unexplored[24–27].

Given that maternal-behaviour-relevant cells in the MPOA are mainly inhibitory and brain lesions that impair parental behaviours sometimes increase infanticide and vice versa[19,24,25,28,29], it was hypothesized that the maternal care circuit and infanticide circuit might counteract each other through reciprocal inhibition[2,5]. On the basis of this hypothesis, we systematically manipulated regions directly connected with the MPOA and identified multiple brain areas that robustly promote negative pup-directed behaviours in female mice. We further examined one of the regions, the bed nucleus of stria terminalis (BNSTpr), in detail, and identified ESR1-expressing cells in the BNSTpr (BNSTpr^{ESR1}) as indispensable for infanticide in female mice.

Regions promoting female infanticide

If the neural circuits driving infanticide and maternal behaviours antagonize each other, reducing the activity in maternal circuit should favour the activation of the infanticide circuit. To test this hypothesis,

[1]Neuroscience Institute, New York University Langone Medical Center, New York, NY, USA. [2]Emotional Brain Institute, Nathan Kline Institute, Child and Adolescent Psychiatry, New York University Langone Medical Center, New York, NY, USA. [3]Department of Psychiatry, New York University Langone Medical Center, New York, NY, USA. [4]Center for Neural Science, New York University, New York, NY, USA. [5]These authors contributed equally: Rongzhen Yan, Luping Yin. ✉e-mail: Long.Mei@nyulangone.org; Dayu.Lin@nyulangone.org

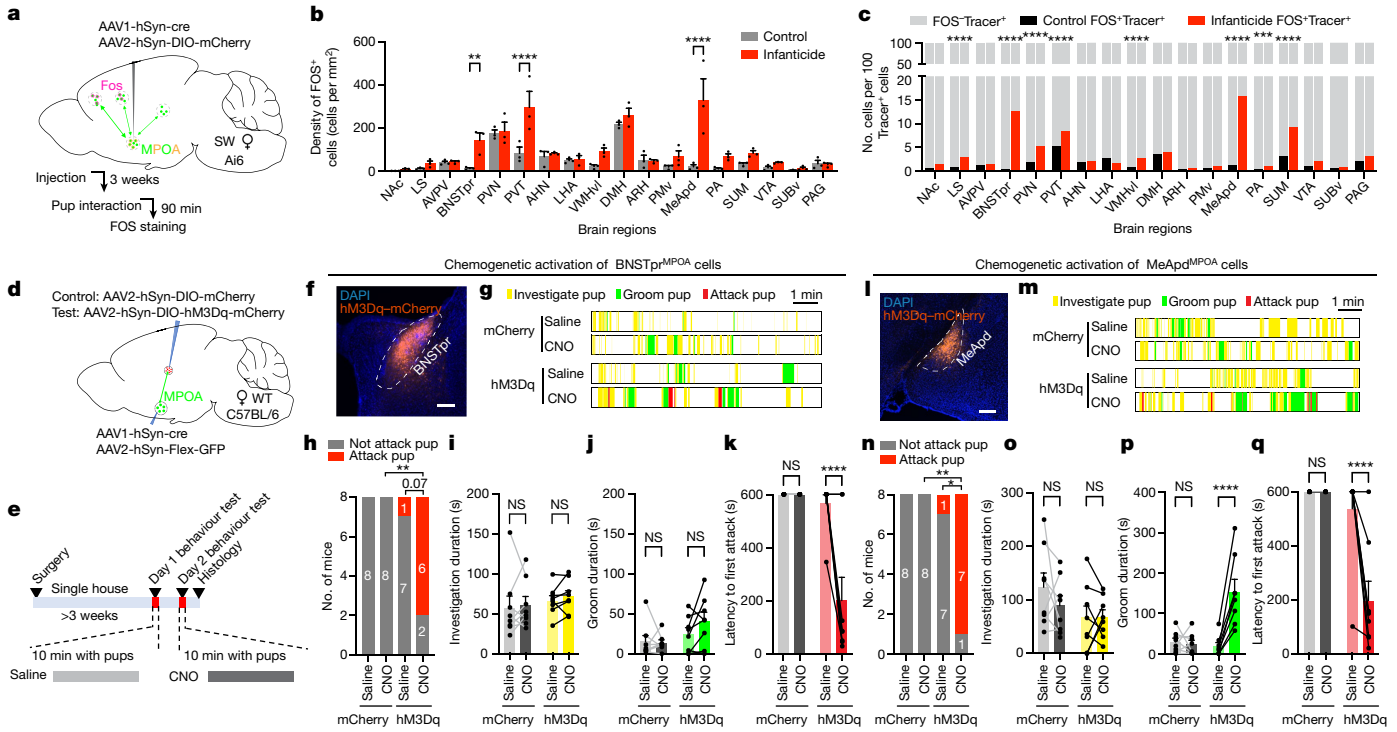

Fig. 1 | Functional screening of brain regions that are relevant for negative pup-directed behaviours in female mice. a, The experimental design to identify infanticide-activated MPOA-connecting cells in female mice. **b**, The density of FOS-expressing cells in MPOA-connecting brain regions in female mice after infanticide or after being left undisturbed (control). $n = 3$ mice per group. LS, lateral septum; NAc, nucleus accumbens; AVPV, anteroventral periventricular nucleus; AHN, anterior hypothalamic nucleus; LHA, lateral hypothalamic area; DMH, dorsomedial nucleus of the hypothalamus; ARH, arcuate hypothalamic nucleus; PA, posterior amygdala; PAG, periaqueductal grey; SUBv, ventral subiculum; VTA, ventral tegmental area. **c**, The total number of FOS$^+$Tracer$^+$ and FOS$^-$Tracer$^+$ cells per 100 Tracer$^+$ cells in MPOA-connecting brain regions across all infanticide and control female mice. **d**, The experimental design to chemogenetically activate MPOA-connecting brain regions. **e**, The experimental timeline. **f**, Representative histology images showing hM3Dq–mCherry expression (red) in BNSTpr^{MPOA} cells. Blue, DAPI. **g**, Representative raster plots showing pup-directed behaviours after saline or CNO injection in mCherry and hM3Dq mice. **h**, The number of female mice that attack or not after saline or CNO injection in mCherry and hM3Dq mice. **i**–**k**, Investigating pup duration (**i**), grooming pup duration (**j**) and latency to attack pups (**k**) after saline or CNO injection in mCherry and hM3Dq mice. Each line represents one animal. If no behaviour of interest was observed during the test, the latency is 600 s. **l**–**q**, As described in **f**–**k**, respectively, but showing that chemogenetic activation of MeApd^{MPOA} cells increases infanticide and pup grooming. For **i**–**k** and **o**–**q**, data are mean ± s.e.m. Statistical analysis was performed using Fisher's exact tests based on the raw FOS$^+$Tracer$^+$ and FOS$^-$Tracer$^+$ cell numbers for each brain region (**c**), McNemar's tests for the saline versus CNO comparison and Fisher's exact test for mCherry versus hM3Dq comparison (**h** and **n**), and two-way repeated-measures analysis of variance (rmANOVA) (**b**,**i**,**o** and **p**) or mixed-effects analysis (**j**,**k** and **q**) followed by adjustment for multiple comparisons. All tests were two-sided; $^{**}P < 0.01$; $^{***}P < 0.001$; $^{****}P < 0.0001$. Details of the statistical analysis are provided as Source Data. Scale bars, 200 µm (**f** and **l**).

we ablated MPOA^{ESR1} neurons and found that the manipulation caused 7 out of 8 virgin non-infanticidal female mice to attack pups without altering pup investigation (Extended Data Fig. 1a–g). Furthermore, we chemogenetically inhibited MPOA^{ESR1} neurons using hM4Di and observed qualitatively similar results: whereas no animal attacked pups after saline injection, all hM4Di female mice but no mCherry female mice showed infanticide after CNO injection (Extended Data Fig. 1h–n). These results support the hypothesis that MPOA has an important role in antagonizing infanticide.

We next aimed to identify MPOA-connecting regions that are activated during infanticide. To achieve this goal, we first searched for female mice showing spontaneous infanticide behaviour. As previously reported, infanticide is rare in adult C57BL/6 female mice[14,15,30]—only 2 out of 165 virgin C57BL/6 female mice attacked pups in our study. By contrast, approximately one-third (50 out 146) of virgin Swiss Webster (SW) female mice attacked and killed pups, making SW mice a suitable animal model for studying the female infanticide circuit in the laboratory.

Next, we identified regions upstream or downstream of the MPOA by injecting high titre (>1×10^{13}) AAV1-Syn-cre[31] into the MPOA of Ai6[32] SW female mice (Extended Data Fig. 2a). MPOA-connecting cells were widely distributed in the brain, including 18 regions containing more than 1% of total labelled cells (Extended Data Fig. 2b–d). Half (9 out of 18) of the highly connected regions were within the hypothalamus and collectively contributed to 69% of total labelled cells (Extended Data Fig. 2d). Outside of the hypothalamus, the densely labelled cells were found in the lateral septum, nucleus accumbens, paraventricular thalamus (PVT), BNSTpr, MeApd, posterior amygdala, ventral subiculum, ventral tegmental area and periaqueductal grey (Extended Data Fig. 2d).

The BNSTpr, PVT and MeApd showed a significantly higher number of FOS$^+$ cells in female mice after infanticide than in single-housed undisturbed female mice (Fig. 1a,b). When we considered only MPOA-connecting cells (Tracer$^+$), infanticide significantly increased FOS expression in the lateral septum, BNSTpr, PVT, paraventricular nucleus (PVN), ventrolateral part of the ventromedial hypothalamus (VMHvl), MeApd, posterior amygdala and supramammillary nucleus (SUM) Tracer$^+$ cells (Fig. 1c), although FOS expression in lateral septum, PVN and posterior amygdala Tracer$^+$ cells was high even after maternal behaviours (Extended Data Fig. 2e–i). On the basis of the FOS expression pattern and MPOA connectivity, we decided to chemogenetically activate MPOA-connecting cells in the BNSTpr, MeApd, VMHvl, PVN,

PVT and SUM during pup interaction. We also included the ventral premammillary nucleus (PMv) in our manipulation list, given its function in intermale aggression[33,34]. As we aimed to identify regions that enhance infanticide, we used C57BL/6 female mice for this experiment given their near-zero spontaneous infanticide.

Notably, pharmacogenetic activation of MPOA-connecting BNSTpr (BNSTpr^{MPOA}) or MeApd (MeApd^{MPOA}) cells elicited repeated attack towards pups in the majority of tested C57BL/6 female mice (Fig. 1d–h,k,l–n,q), while the total duration of pup investigation did not change (Fig. 1i,o). Activating the MeApd^{MPOA} cells, but not BNSTpr^{MPOA} cells, also increased pup grooming (Fig. 1j,p)—a behavioural change that was observed previously during optogenetic activation of MeApd GABAergic cells[27]. Animals that expressed mCherry in MeApd^{MPOA} or BNSTpr^{MPOA} cells showed no infanticide after either saline or CNO injection (Fig. 1f–q).

When the MPOA-connecting VMHvl (VMHvl^{MPOA}) cells were chemogenetically activated, the test female mice avoided the pups, but none showed infanticide (Extended Data Fig. 3a–c). When the MPOA-connecting SUM cells were activated, pup grooming decreased slightly, while other behaviours did not change significantly (Extended Data Fig. 4d). Activating MPOA-connecting PVT, PVN and PMv cells caused no significant behaviour change towards the pups (Extended Data Fig. 4e–g). These results suggest that pup-directed behaviours, including pup avoidance, pup grooming and infanticide, are mediated by different combinations of brain regions. BNSTpr^{MPOA} cells could have an important and specific role in driving infanticide.

BNSTpr^{MPOA} activation drives infanticide

To understand whether the BNSTpr^{MPOA} cells drive infanticide acutely or only increase the likelihood of its expression, we optogenetically activated BNSTpr^{MPOA} cells bilaterally in virgin C57BL/6 female mice (Extended Data Fig. 4a–c). After light stimulation (20 ms, 20 Hz, 20 s), even at the lowest intensity (0.5 mW), 10 out of 11 ChR2-expressing female mice attacked pups after contact in approximately 65% of trials, whereas no GFP-expressing female mice attacked the pups (Extended Data Fig. 4d–i). The increase in attack probability was almost immediate after light onset and the average latency to attack was approximately 3 s (Extended Data Fig. 4g,j). Increasing the light intensity did not change the induced behaviour qualitatively, although there was a trend of decrease in light-evoked attack probability (Extended Data Fig. 4d–j).

Stress can negatively affect maternal behaviours[35,36], and several BNST subdivisions (though not BNSTpr) were shown to modulate stress and anxiety[37–39]. To understand whether BNSTpr^{MPOA} stimulation-evoked infanticide is due to an increase in anxiety, we examined light-evoked behavioural changes in a real-time place preference test (RTPP) and an elevated plus maze test (EPM) (Extended Data Fig. 4k–n). We found that activation of BNSTpr^{MPOA} increased the fraction of time spent on the stimulated side (Extended Data Fig. 4l) and open arms (Extended Data Fig. 4n), suggesting that BNSTpr^{MPOA} stimulation is not aversive or anxiogenic. Thus, the stimulation-induced infanticide is not secondary to an increase in stress.

BNSTpr^{ESR1} activation drives infanticide

ESR1 is expressed widely in regions that are important for social behaviours[40]. ESR1^{+} cells in the VMHvl, MPOA and posterior amygdala were found to be preferentially involved in social behaviours compared with ESR1^{-} cells[18,41–43]. Within the BNST, ESR1 is concentrated in the BNSTpr. Its expression is lower in male mice compared with in female mice regardless of the reproductive state of the female mice[44] (Extended Data Fig. 5a–c). Thus, we next investigated the possibility that ESR1 is a relevant molecular marker for infanticide cells in the BNSTpr. Immunostaining revealed that ESR1 is expressed in approximately half of the BNSTpr cells (Extended Data Fig. 5d–f). Notably, over 90% of infanticide-induced FOS cells overlap with ESR1 cells, and approximately 85% of MPOA-connecting BNSTpr cells are ESR1^{+} (Extended Data Fig. 5d–f). Within the BNSTpr^{ESR1} cells, approximately 15% express infanticide-induced FOS (Extended Data Fig. 5f). Thus, ESR1 preferentially marks the BNSTpr population activated by infanticide and largely encompasses the cells connected with MPOA.

We next optogenetically activated BNSTpr^{ESR1} neurons bilaterally in virgin Esr1-2A-cre C57BL/6 female mice and found that the manipulation induced pup attack even more reliably and quickly than BNST^{MPOA} cell activation (Fig. 2a–l). Regardless of the light intensity, infanticide was induced in all tested female mice (8 out of 8) and in 92% of total pup interaction stimulation trials with an average latency of 1 s (Fig. 2k–l). No test animals showed spontaneous pup attack without light, and no GFP control animals attacked the pups during the entire test session (Fig. 2d–l). We further examined whether BNSTpr^{ESR1} activation can override the maternal behaviours in mothers. Indeed, light stimulation induced reliable infanticide in all lactating female mice (6 out of 6), even towards their own pups, whereas all mothers quickly retrieved and cared for pups after sham stimulation (Fig. 2h–l).

To understand whether the function of BNSTpr^{ESR1} cells is strain specific, we carried out the optogenetic activation in non-infanticidal Esr1-2A-cre female mice in the SW background and observed similar results in both virgin and lactating female mice (Extended Data Fig. 5g–m). These results indicate that BNSTpr^{ESR1} cells are sufficient to drive infanticide in female mice regardless of the reproductive state and genetic background of the mice.

BNSTpr^{ESR1} is necessary for infanticide

To determine whether BNSTpr^{ESR1} neurons are necessary for infanticide in female mice, we inhibited BNSTpr^{ESR1} cells using h4MDi in virgin Esr1-2A-cre SW female mice (Fig. 2m–o). For the nine spontaneously infanticidal hM4Di female mice, all attacked and killed pups after saline injection, whereas only one did so after CNO injection and six out of nine female mice even retrieved the pups (Fig. 2p–s). For the five h4MDi female mice that neither attacked nor retrieved pups, four out five female mice retrieved pups after CNO injection, whereas none did so after saline injection (Extended Data Fig. 6a–c). CNO injection did not change the total duration of pup investigation (Extended Data Fig. 6d). Similarly, inactivating BNSTpr^{ESR1} cells in lactating female mice shortened the latency to retrieve all pups (Extended Data Fig. 6e–h). Together, these results support that BNSTpr^{ESR1} cells not only drive infanticide but also suppress maternal behaviours in female mice.

BNSTpr^{ESR1} and MPOA^{ESR1} mutually inhibit

Inhibiting MPOA^{ESR1} cells impairs maternal behaviour and promotes infanticide, whereas inhibiting BNSTpr^{ESR1} cells impairs infanticide and promotes maternal behaviours. These results strongly suggest an antagonistic relationship between these two populations, possibly through mutual inhibition. To test this hypothesis, we first examined the projection patterns of BNSTpr^{ESR1} and MPOA^{ESR1} cells by virally expressing GFP in these cells. We found dense terminal fields from BNSTpr^{ESR1} cells in the ESR1-enriched region in the MPOA and vice versa (Fig. 3a–c,f–h). A survey of the GFP fibres throughout the brain revealed that the MPOA represents one of the major downstream regions of the BNSTpr^{ESR1}, whereas the BNSTpr receives moderate input from MPOA^{ESR1} cells (Fig. 3d,e,i,j).

We then performed ChR2-assisted circuit mapping on brain slices to investigate the synaptic connections between MPOA^{ESR1} to BNSTpr^{ESR1} cells (Fig. 3k,s). We found that BNSTpr^{ESR1} terminal activation evoked inhibitory postsynaptic currents (oIPSCs) in more than 90% (20 out of 22) of MPOA^{ESR1} neurons, including two neurons

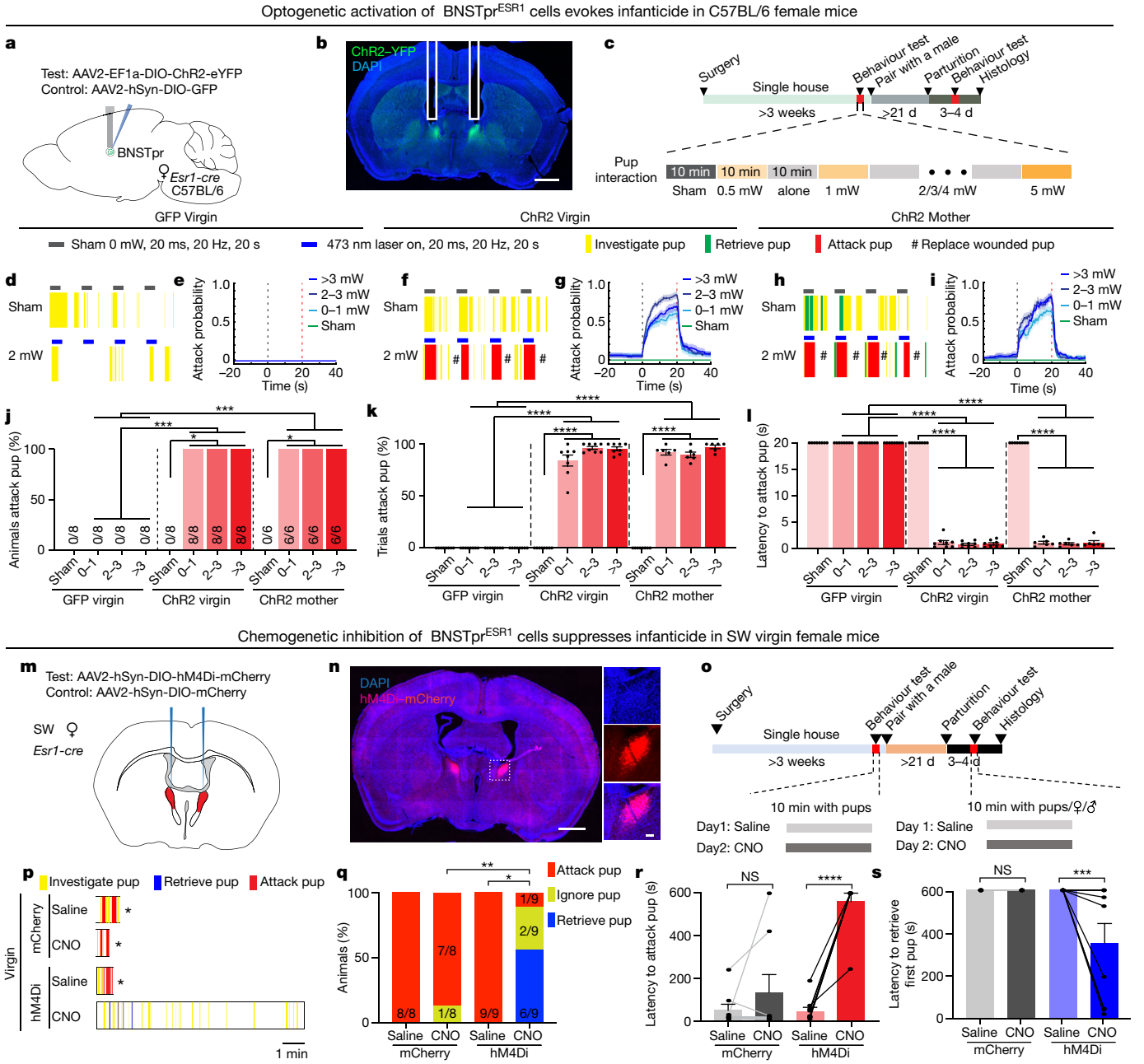

Fig. 2 | BNSTpr^{ESR1} neurons are sufficient and necessary for female infanticide. **a**, The experimental design. **b**, Representative histology showing ChR2–eYFP expression. The white lines indicate the fibre tracks. Scale bar, 1 mm. **c**, The experimental timeline. **d**–**i**, Experiments in GFP virgin (**d**,**e**), ChR2 virgin (**f**,**g**) and ChR2 mother (**h**,**i**) mice. **d**,**f**,**h**, Raster plots showing pup-directed behaviours during sham and light stimulation. The hash symbol (#) indicates that a pup was replaced. **e**,**g**,**i**, Post-event histograms (PETHs) of attack pup probability aligned to sham and light onset. Only trials with female–pup contact were included. The dashed lines mark the light period. **j**, The percentage of animals that attacked pups. **k**, The percentage of trials showing pup attack. Only trials with female–pup contact were included. **l**, The average latency to attack pup after pup encounter following sham or light stimulation. **m**, The experimental design to inhibit BNSTpr^{ESR1} cells. The brain illustration is based on a reference atlas from https://atlas.brain-map.org/. **n**, Representative histology showing hM4Di–mCherry expression. Scale bars, 1 mm (left) and 100 µm (right). **o**, The experimental timeline. **p**, Raster plots showing pup-directed behaviours after CNO or saline injection. Where indicated by an asterisk, wounded pups were removed and recording was stopped. **q**, The percentage of spontaneously infanticidal virgin female mice that attack, ignore or retrieve pups after saline or CNO injection. **r**,**s**, Latency to attack (**r**) and retrieve pups (**s**) after saline or CNO injection. Latency equals 600 s if the behaviour did not occur during the test. For **k**,**l**,**r** and **s**, each dot or line represents one animal. For **e**,**g**,**i**,**k**,**l**,**r** and **s**, data are mean ± s.e.m. Statistical analysis was performed using Fisher's exact tests for between-animal comparisons and McNemar's tests for within-animal comparisons (**q**), and mixed-effects analysis followed by correction for multiple comparisons (**k**,**l**,**r** and **s**). All tests were two-sided; *$P < 0.05$. $n = 8$ (GFP), $n = 8$ (ChR2 virgin) and $n = 6$ (ChR2 mother) (**e**,**g**,**i**,**j**–**l**) and $n = 8$ (mCherry) and $n = 9$ (hM4Di) (**q**–**s**) mice. Details of the statistical analysis are provided as Source Data.

showing both oIPSCs and evoked excitatory postsynaptic currents (oEPSCs) (Fig. 3l). The oIPSC was large (mean ± s.e.m., 930 ± 166 pA) and monosynaptic as it was blocked by tetrodotoxin (TTX) and rescued by TTX and 4-aminopyridine (4-AP) (Fig. 3m,n). The oIPSC is mediated mainly by $GABA_A$ receptors and, to a lesser extent, by glycine receptors—the $GABA_A$ receptor antagonist, gabazine, completely

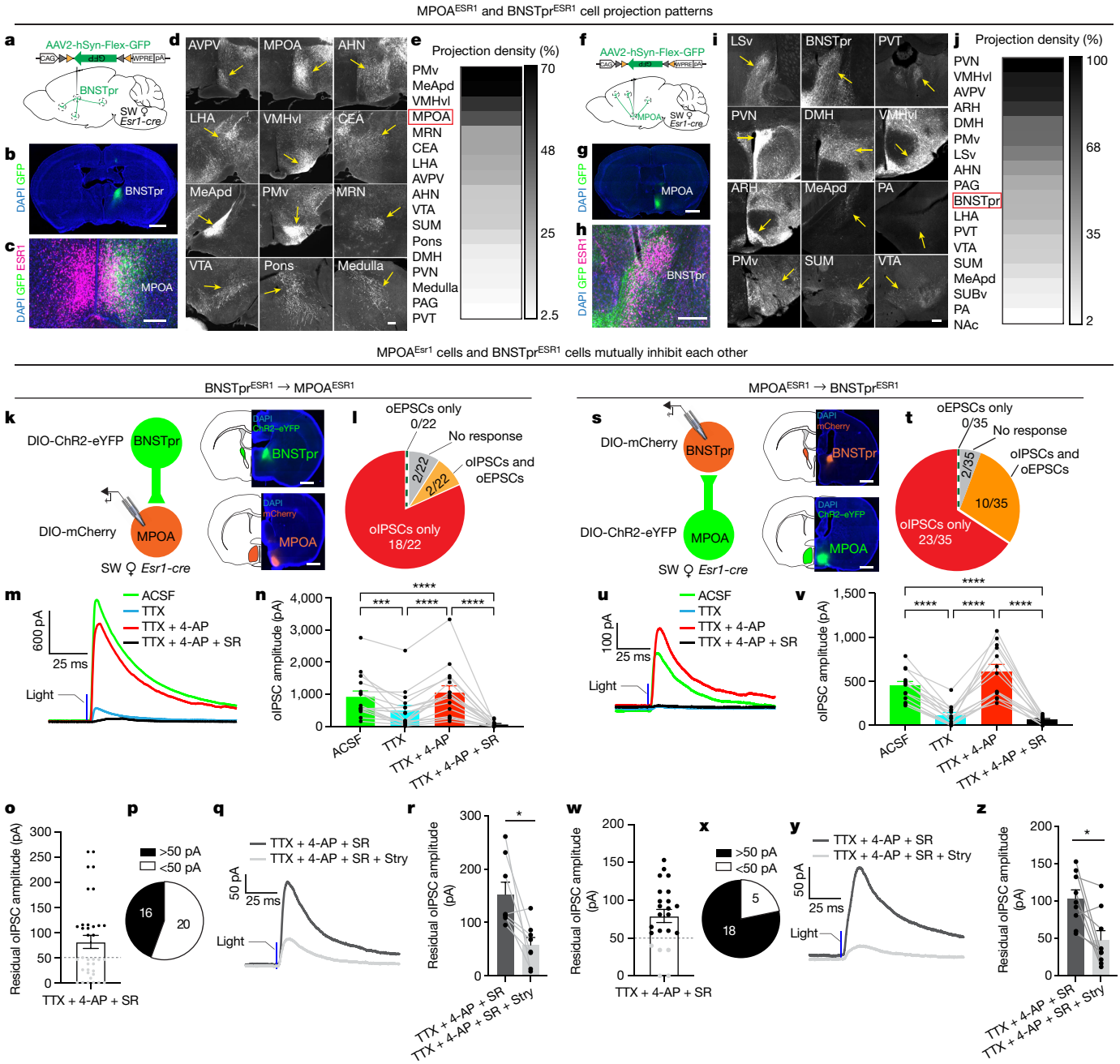

Fig. 3 | Mutual inhibition between BNSTpr^{ESR1} and MPOA^{ESR1} cells. **a**, Anterograde tracing of BNSTpr^{ESR1} cells. **b**, Representative GFP expression in BNSTpr^{ESR1} cells. **c**, Representative GFP-expressing BNSTpr^{ESR1} terminals (green) in the MPOA, and ESR1 staining (magenta). **d**, Representative GFP-expressing BNSTpr^{ESR1} terminals in various regions. **e**, The brain-wide projection density of BNSTpr^{ESR1} cells, normalized to the BNSTpr fluorescence intensity. $n = 4$ mice. **f**–**j**, Experiments as described in **a**–**e**, respectively, but showing MPOA^{ESR1} cell projection patterns. $n = 4$ mice. **k**,**s**, Schematics of ChR2-assisted circuit mapping of the BNSTpr^{ESR1} to MPOA^{ESR1} (**k**) and MPOA^{ESR1} to BNSTpr^{ESR1} (**s**) pathways and representative histological images. The brain atlases were reproduced based on a reference atlas from https://atlas.brain-map.org/. **l**,**t**, The synaptic response patterns of MPOA^{ESR1} cells to BNSTpr^{ESR1} terminal activation (**l**; 22 cells from 3 mice) and BNSTpr^{ESR1} cells to MPOA^{ESR1} terminal activation (**t**; 35 cells from 3 mice). **m**,**u**, Representative oIPSCs from MPOA^{ESR1} cells (**m**) and BNSTpr^{ESR1} cells (**u**) with different blockers. SR, gabazine. **n**,**v**, The oIPSC amplitude with different blockers of MPOA^{ESR1} cells (**n**) and BNSTpr^{ESR1} cells (**v**). Statistical analysis was performed using a mixed-effects analysis followed by correction for multiple comparisons. $n = 16$ cells from 4 mice (**n**) and 13 cells from 5 mice (**v**); each line represents one cell. **o**,**w**, The oIPSC amplitude of MPOA^{ESR1} (**o**) and BNSTpr^{ESR1} (**w**) cells after applying a TTX, 4-AP and gabazine mixture. $n = 36$ cells from 8 mice (**o**) and 23 cells from 9 mice (**w**). **p**,**x**, The number of MPOA^{ESR1} (**p**) and BNSTpr^{ESR1} (**x**) cells with a residual oIPSC of >50 pA or <50 pA after applying a mixture of TTX, 4-AP and gabazine. **q**,**y**, Representative oIPSCs of MPOA^{ESR1} (**q**) and BNSTpr^{ESR1} (**y**) cells before and after applying strychnine (Stry)—a glycine receptor antagonist. **r**,**z**, The oIPSC amplitude of MPOA^{ESR1} (**r**) and BNSTpr^{ESR1} (**z**) cells before and after applying strychnine. Statistical analysis was performed using a two-sided paired signed-rank test. $n = 8$ cells from 4 mice (**r**); 9 cells from 4 mice (**z**). For **n**,**v**,**o**,**r**,**v**,**w** and **z**, data are mean ± s.e.m. Details of the statistical analysis are provided as Source Data. Scale bars, 1 mm (**b**,**g**,**k** and **s**) and 200 µm (**c**,**d**,**h** and **i**).

blocked oIPSCs in 56% (20 out of 36) of cells (Fig. 3m–p) and the residual oIPSCs were further blocked by the glycine receptor inhibitor strychnine (Fig. 3q,r).

Similarly, 94% (33 out of 35) of BNSTpr^{ESR1} cells showed oIPSCs after MPOA^{ESR1} terminal stimulation, including 10 cells that showed both oIPSCs and oEPSCs (Fig. 3t). The higher proportion of cells showing

oEPSCs after MPOA^{ESR1} to BNSTpr^{ESR1} stimulation in comparison to after BNSTpr^{ESR1} to MPOA^{ESR1} stimulation is consistent with the fact that BNSTpr^{ESR1} cells are nearly exclusively GABAergic, whereas approximately a quarter of MPOA^{ESR1} cells are glutamatergic[18,45]. The oIPSCs can be blocked by bath application of TTX and rescued by TTX and 4-AP, suggesting the monosynaptic nature of the connection (Fig. 3u,v). The oIPSCs are mediated mainly by the $GABA_A$ receptor and, to a lesser extent, by the glycine receptor (Fig. 3u–z). These results suggested that BNSTpr^{ESR1} and MPOA^{ESR1} neurons form strong reciprocal inhibitory connections.

MPOA^{ESR1} to BNSTpr pathway suppresses infanticide

We next expressed ArchT in MPOA^{ESR1} cells and optogenetically inhibited the MPOA^{ESR1} terminals in the BNSTpr in virgin non-infanticidal Esr1-2A-cre SW female mice (Fig. 4a and Extended Data Fig. 7a,b). Slice recording confirmed that yellow light effectively blocked the inhibitory synaptic transmission from ArchT-expressing axon terminals (Extended Data Fig. 8). We found that inhibiting MPOA^{ESR1}–BNSTpr projection significantly increased pup attack (Fig. 4b–e). After light delivery, five out of six ArchT female mice attacked pups with a latency of approximately 1 min, typically after a period of pup investigation, whereas none of the mCherry control animals attacked pups (Fig. 4b–d). Given the long latency of light-induced attack, this result suggests that removing the inhibition from MPOA^{ESR1} to BNSTpr increased the probability of infanticide but did not trigger attack action acutely, as observed during BNSTpr^{ESR1} activation.

Next, we expressed ChrimsonR in MPOA^{ESR1} cells and activated MPOA^{ESR1} to BNSTpr projection in infanticidal virgin SW female mice (Fig. 4f). Notably, all ChrimsonR female mice stopped attacking pups, and three out seven mice showed pup retrieval (Fig. 4g–j). However, histological analysis revealed FOS induction in the MPOA after light delivery to the BNSTpr, suggesting activation of the MPOA^{ESR1} cell body possibly due to backpropagation of action potentials or disinhibition after BNSTpr inhibition (Extended Data Fig. 7c,d,f). To prevent MPOA cell body activation, we co-injected Cre-dependent hM4Di-mCherry and ChR2-eYFP viruses into the MPOA and injected CNO 30 min before optogenetic activation of MPOA^{ESR1}–BNSTpr projection (Fig. 4f). Indeed, CNO effectively eliminated terminal stimulation-induced FOS increase in the MPOA (Extended Data Fig. 7c,e,f). Under this condition, light activation of MPOA^{ESR1}–BNSTpr terminals suppressed infanticide but did not increase maternal behaviours (Fig. 4g–j). Thus, MPOA^{ESR1} input to the BNSTpr can bidirectionally modulate infanticidal behaviour—an increase in MPOA^{ESR1} input suppresses infanticide, whereas a decrease in input facilitates infanticide.

BNSTpr^{ESR1} to MPOA pathway suppresses maternal care

When we optogenetically inhibited BNSTpr^{ESR1} input to the MPOA in spontaneously infanticidal female mice, we observed behavioural changes opposite to that during MPOA^{ESR1}–BNSTpr pathway inhibition (Fig. 4k–o and Extended Data Fig. 7g,h). Whereas all mCherry control female mice showed infanticide, only one out of six ArchT female mice briefly attacked the pup with light delivery, suggesting that BNSTpr^{ESR1} inhibition onto MPOA is functionally important to ensure the expression of infanticide (Fig. 4k–o).

When we optogenetically activated the BNSTpr^{ESR1}–MPOA pathway in non-infanticidal female mice, maternal behaviours were suppressed, and all female mice (five out of five) attacked the pups repeatedly (Fig. 4p–t). However, BNSTpr^{ESR1}–MPOA terminal stimulation induced strong FOS expression in the BNSTpr (Extended Data Fig. 7i,j,l). We therefore chemogenetically inhibited BNSTpr^{ESR1} cell bodies while optogenetically activating BNSTpr^{ESR1}–MPOA terminals (Fig. 4p and Extended Data Fig. 7k,l). Under this scenario, we found reduced maternal behaviours but no increase in infanticide, suggesting that the BNSTpr^{ESR1}–MPOA pathway mainly has a role in suppressing maternal behaviours (Fig. 4q–t). Together, these results support the hypothesis that BNSTpr^{ESR1} and MPOA^{ESR1} directly antagonize each other through mutual inhibition. The relative activity between these two regions determines the female behaviours towards the pups.

BNSTpr^{ESR1} versus MPOA^{ESR1} cell responses

We next examined why a pup-killing virgin female mouse suddenly cares for the young after becoming a mother. Our functional results suggest that this behaviour switch could be due to a change in the relative activity of BNSTpr^{ESR1} and MPOA^{ESR1} cells. Thus, we next performed longitudinal population Ca^{2+} recordings to reveal potential response changes of BNSTpr^{ESR1} and MPOA^{ESR1} cells during motherhood (Fig. 5a–g). Over 90% GCaMP6f^{+} cells express ESR1, confirming that the fluorescence signal largely came from ESR1 cells (Fig. 5c).

During the first pup contact after its introduction, we observed a sharp increase in the Ca^{2+} signal of BNSTpr^{ESR1} cells in hostile virgin female mice but not in lactating female mice (Fig. 5h,i,m). During subsequent pup approach, the Ca^{2+} signal did not significantly increase regardless of the reproductive state of the female mice (Fig. 5j,n,o). During close pup investigation, Ca^{2+} increased only slightly (Fig. 5k,n,o). When the hostile female attacked a pup, BNSTpr^{ESR1} cell activity increased strongly and was maintained at a high level until the end of the attack (Fig. 5h (top), 5l (top) and 5n). By contrast, the cell activity increased only slightly during pup retrieval in mothers (Fig. 5h (bottom), 5l (bottom) and 5n). The average response of BNSTpr^{ESR1} cells during infanticide is significantly higher than that during retrieval (Fig. 5o). Overall, BNSTpr^{ESR1} cells showed higher responses to pups in hostile virgins than mothers (Fig. 5m–o). Control animals that expressed GFP in BNSTpr^{ESR1} or MPOA^{ESR1} cells showed no response during any pup-directed behaviours, suggesting the responses of GCaMP6 animals are contributed minimally by movement artifacts (Extended Data Fig. 9a–n). Moreover, BNSTpr^{MPOA} cell responses during pup interaction were found to be similar to BNSTpr^{ESR1} cell responses (Extended Data Fig. 9o–y).

The response pattern of MPOA^{ESR1} cells is distinct from that of BNSTpr^{ESR1} cells (Fig. 5p–w). The activity increase during pup entry was the highest in mothers and lowest in hostile virgins (Fig. 5p,q,u). In virgin hostile female mice, MPOA^{ESR1} cell activity increased minimally during approach and investigation and not at all during attacking pups (Fig. 5p–t (top) and 5v). In maternal virgin female mice and mothers, the Ca^{2+} signal started to rise when the female mouse approached the pup, continued to increase during investigation and reached maximum during retrieval (Fig. 5p–t (middle and bottom) and 5v). The average response of MPOA^{ESR1} cells during retrieval is significantly higher than during infanticide (Fig. 5w).

To directly compare the temporal dynamics of BNSTpr^{ESR1} and MPOA^{ESR1} cells, we recorded Ca^{2+} signals from these two populations simultaneously (Extended Data Fig. 10a–e). During pup approach and investigation, MPOA^{ESR1} cell activity rose earlier than that of BNSTpr^{ESR1} cells in both hostile virgin female mice and mothers, suggesting higher sensitivity of MPOA^{ESR1} cells to pup cues than BNSTpr^{ESR1} cells (Extended Data Fig. 10f–g). At the onset of pup attack, MPOA^{ESR1} cell activity decreased while BNSTpr^{ESR1} cell activity continuously increased (Extended Data Fig. 10f1–h1). Thus, at the offset of attack, MPOA^{ESR1} cell activity was below the baseline, whereas BNSTpr^{ESR1} cell activity was above the baseline (Extended Data Fig. 10g1). In mothers, MPOA^{ESR1} cells were highly active during pup investigation and retrieval, whereas BNSTpr^{ESR1} cell activity stayed low throughout pup-directed behaviours (Extended Data Fig. 10f2–h2). The ratio of overall activity between BNSTpr^{ESR1} and MPOA^{ESR1} cells (BNSTpr^{ESR1}/MPOA^{ESR1}) during pup interaction was >1 in hostile virgins and <1 in mothers (Extended Data Fig. 10i).

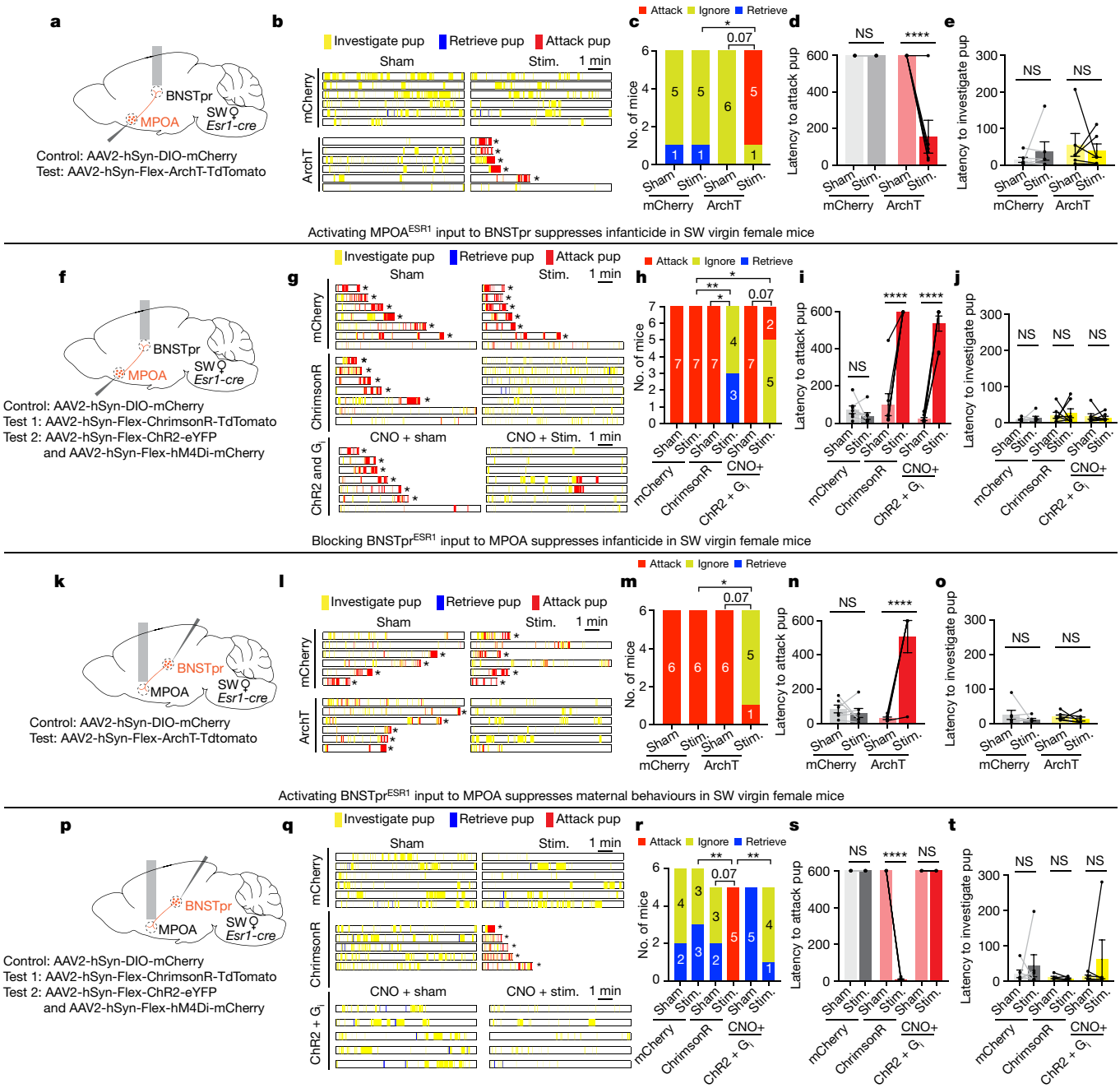

Fig. 4 | BNSTpr^{ESR1} and MPOA^{ESR1} cells antagonize each other functionally through their reciprocal projections. a, The experimental design to optogenetically inactivate the MPOA^{ESR1} to BNSTpr pathway. **b**, Raster plots showing pup-directed behaviours in mCherry and ArchT female mice during sham or 5 mW continuous yellow light delivery. Where indicated by an asterisk, wounded pups were removed and recording was stopped. **c**, The number of mCherry and ArchT female mice that attacked, ignored or retrieved pups during sham or light stimulation. **d**,**e**, The latency to attack (**d**) and investigate (**e**) the pup during sham and light delivery in mCherry and ArchT female mice. The latency equals 600 s if the behaviour of interest did not occur during the test. $n = 6$ mice per group. **f**, The experimental design to optogenetically activate the BNSTpr^{ESR1} to MPOA pathway with or without BNSTpr^{ESR1} chemogenetic inhibition. **g**, Raster plots showing pup-directed behaviours in various groups during sham or light delivery. Where indicated by an asterisk, wounded pups were removed and recording was stopped. **h**, The number of female mice in each group that attacked, ignored or retrieved pups during sham or light delivery. **i**,**j**, The latency to attack (**i**) and investigate (**j**) the pup during sham or light delivery in control and test female mice. $n = 7$ mice per group. **k**–**o**, Experiments as in **a**–**e**, respectively, but showing that optogenetic inactivation of the BNSTpr^{ESR1} to MPOA pathway in spontaneously infanticidal virgin SW female mice suppresses infanticide. $n = 6$ mice per group. **p**–**t**, Experiments as in **f**–**j**, respectively, but showing that optogenetic activation of the BNSTpr^{ESR1} to MPOA pathway suppresses maternal behaviours. $n = 6$ (mCherry), $n = 5$ (ChrimsonR) and $n = 5$ (ChR2 + G_i) mice. For **d**,**e**,**i**,**j**,**n**,**o**,**s** and **t**, data are mean ± s.e.m. Statistical analysis was performed using Fisher's exact tests for comparing behaviour outcomes (attack versus not attack) between control and test groups with the same light treatment and McNemar's test for comparisons between light and sham trials within a group (**c**,**h**,**m** and **r**), and mixed-effects analysis followed by correction for multiple comparisons (**d**,**e**,**i**,**j**,**n**,**o**,**s** and **t**). All tests were two-sided. Details of the statistical analysis are provided as Source Data.

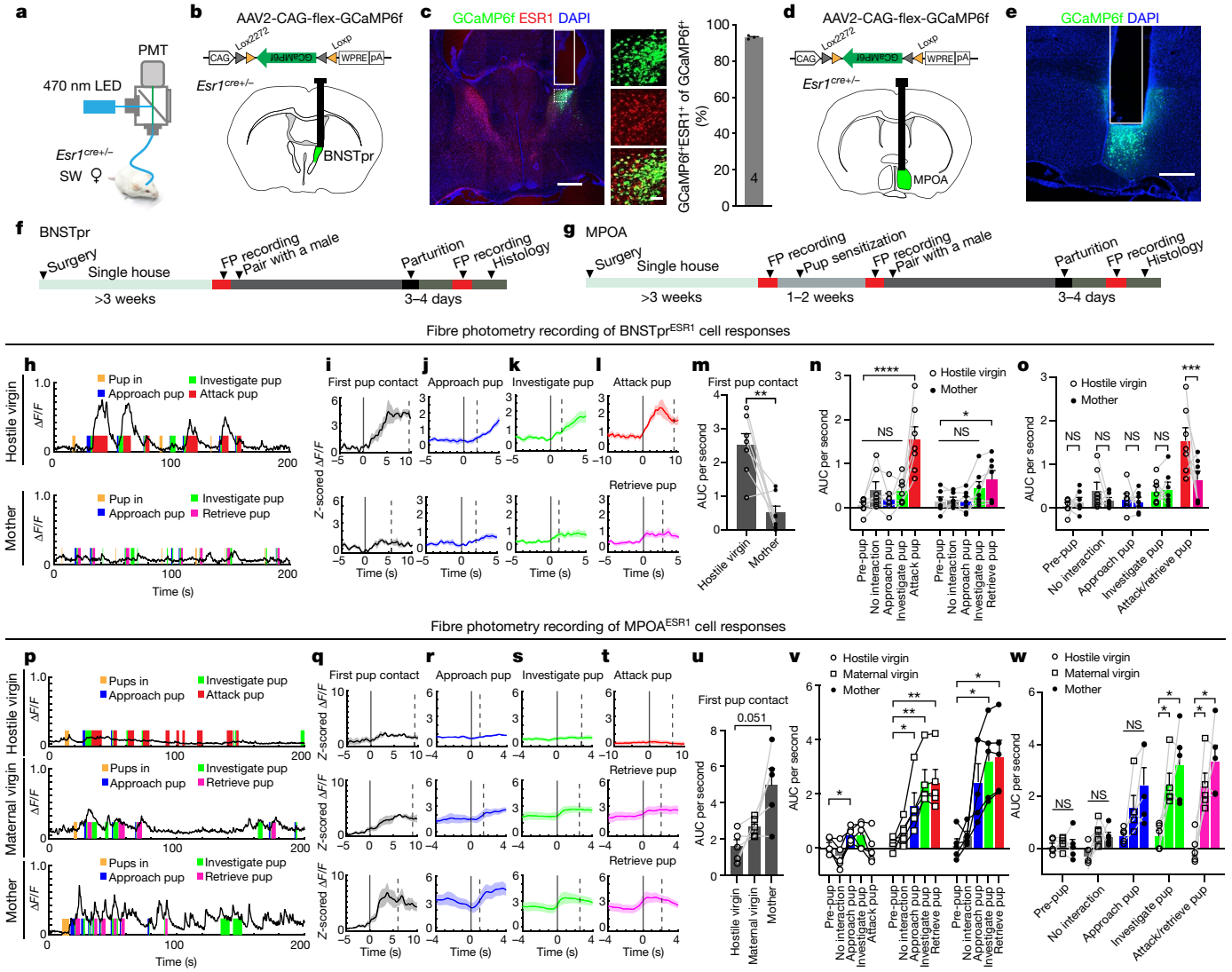

Fig. 5 | Distinct responses of BNSTpr^{ESR1} and MPOA^{ESR1} cells during female infanticide and maternal care. a, The fibre photometry set-up. **b**,**d**, The viral construct and the targeted brain regions. The brain illustration was produced based on a reference atlas from https://atlas.brain-map.org/. **c**, A representative image of four mice showing the fibre track in the BNSTpr (white line), and the overlap between ESR1 staining (red) and GCaMP6f (green). An enlarged view of the boxed area is shown on the right. The percentage of GCaMP6f cells expressing ESR1 is shown. $n = 4$ recorded mice. Scale bars, 500 µm (left) and 50 µm (right). **e**, Representative GCaMP6f expression (green) and fibre track (white line) in the MPOA of four mice. Scale bar, 200 µm. **f**,**g**, The experimental timelines for BNSTpr cells (**f**) and MPOA cells (**g**). **h**, Representative Δ*F*/*F* traces of BNSTpr^{ESR1} cells during pup interaction with a hostile virgin female (**h**, top) and a mother (**h**, bottom). **i**–**l**, PETHs of *Z*-scored Δ*F*/*F* of BNSTpr^{ESR1} cells aligned to the onset of the following behaviours: first pup contact (**i**), approach pup (**j**), investigate pup (**k**), and attack pup (**l**, top) and retrieve pup (**l**, bottom). **m**, The average area under the curve (AUC) of the *Z*-scored Δ*F*/*F* during the first pup contact. **n**,**o**, The mean AUC of the *Z*-scored Δ*F*/*F* during various pup-directed behaviours to compare responses across behaviours in hostile virgins and mothers (**n**) and responses of the same behaviour between hostile virgins and mothers (**o**). **p**, Representative Δ*F*/*F* traces of MPOA^{ESR1} cells during pup interaction. **q**–**t**, PETHs of *Z*-scored Δ*F*/*F* of MPOA^{ESR1} cells aligned to the onset of the following pup-directed behaviours: first pup contact (**q**), approach pup (**r**), investigate pup (**s**), and attack pup (**t**, top) and retrieve pup (**t**, middle and bottom). **u**, The mean AUC of the *Z*-scored Δ*F*/*F* during the first pup contact. **v**,**w**, The mean AUC of the *Z*-scored Δ*F*/*F* during various pup-directed behaviours to compare responses across behaviours in hostile virgins, maternal virgins and mothers (**v**) and responses of the same behaviour across female mice under different reproductive states (**w**). For **i**–**o** and **q**–**w**, data are mean ± s.e.m. For **i**–**w** and **q**–**t**, the solid and dashed lines indicate the onset and offset of behaviours, respectively. Statistical analysis was performed using two-sided paired *t*-tests (**m**), one-way rmANOVA with correction for multiple comparisons (**u**), two-way rmANOVA with correction for multiple comparisons (**n** and **o**) and mixed-effects analysis with correction for multiple comparisons (**v** and **w**). $n = 7$ (**i**–**o**) and $n = 5$ (**q**–**w**) mice per group. Details of the statistical analysis are provided as Source Data.

C57BL/6 female mice rarely show infanticide, making it difficult to compare the BNSTpr^{ESR1} and MPOA^{ESR1} cell responses in infanticidal and maternal animals. Nevertheless, the FOS expression pattern in maternal virgin C57BL/6 female mice is similar to that of maternal SW female mice: high in the MPOA and low in the BNSTpr, which is opposite to the pattern observed in infanticidal SW female mice (Extended Data Fig. 10j–l). Together, these results suggest a reverse in the relative activity level between MPOA^{ESR1} and BNSTpr^{ESR1} cells during motherhood.

Excitability changes during motherhood

We next examined what physiological mechanism is responsible for the in vivo response change of BNSTpr^{ESR1} and MPOA^{ESR1} cells

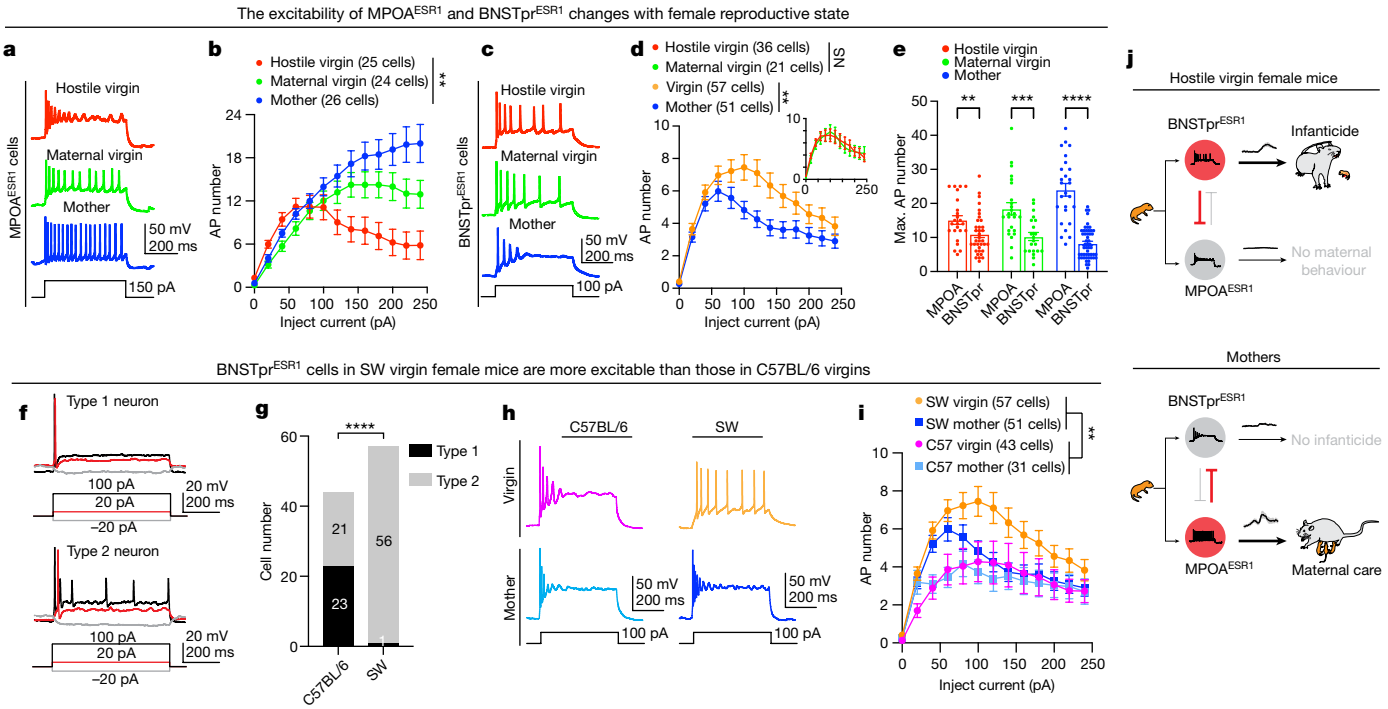

Fig. 6 | BNSTpr^{ESR1} and MPOA^{ESR1} cell excitability varies with the reproductive state and genetic background of female mice. a, Representative recording traces of MPOA^{ESR1} cells. **b**, *F–I* curves of MPOA^{ESR1} cells from hostile virgin (red, 25 cells from 3 mice), maternal virgin (green, 24 cells from 3 mice) and lactating (blue, 26 cells from 3 mice) SW female mice. **c**, Representative recording traces of BNSTpr^{ESR1} cells. **d**, *F–I* curves of BNSTpr^{ESR1} cells from SW virgin female mice (orange, 57 cells from 6 mice) and mothers (blue, 51 cells from 9 mice). Inset: *F–I* curves of BNSTpr^{ESR1} cells from hostile (red, 36 cells from 3 mice) and maternal virgin (green, 21 cells from 3 mice) SW female mice. **e**, The maximum action potential number of MPOA^{ESR1} and BNSTpr^{ESR1} cells from hostile virgin (red, MPOA: 25 cells from 3 mice; BNSTpr: 36 cells from 3 mice), maternal virgin (green, MPOA: 24 cells from 3 mice; BNSTpr: 21 cells from 3 mice) and lactating (blue, MPOA: 24 cells from 3 mice; BNSTpr: 51 cells from 9 mice) SW female mice with maximally 250 pA injected current. **f**, Representative traces showing the spiking patterns of type I and II BNSTpr^{ESR1} cells. **g**, The number of type I and II BNSTpr^{ESR1} cells in C57BL/6 (3 mice) and SW (6 mice) virgin female mice. **h**, Representative recording traces of type II BNSTpr^{ESR1} cells from C57BL/6 and SW virgin female mice and mothers. **i**, *F–I* curves of BNSTpr^{ESR1} cells recorded from C57BL/6 (virgin: 43 cells from 3 mice; mother: 31 cells from 3 mice) and SW (virgin: 57 cells from 6 mice; mother: 51 cells from 9 mice) female mice. **j**, A cartoon summary of the antagonism between the infanticide and maternal circuits and their changes with reproductive states. For **b**,**d**,**e** and **i**, data are mean ± s.e.m. Statistical analysis was performed using mixed-effects analysis with correction for multiple comparisons (**b**,**d** and **i**), Mann–Whitney *U*-tests (hostile virgin and mother) or unpaired *t*-tests (maternal virgin) (**e**) and Fisher's exact tests (**g**). All tests were two-sided. Details of the statistical analysis are provided as Source Data.

during motherhood. To address this question, we performed in vitro current-clamp recording of MPOA^{ESR1} and BNSTpr^{ESR1} cells from dioestrus hostile virgin, dioestrus maternal virgin and lactating (postpartum day 3) SW female mice and found distinct state-dependent changes in MPOA^{ESR1} and BNSTpr^{ESR1} cell excitability (Fig. 6a–e). MPOA^{ESR1} cells in hostile virgin female mice were prone to depolarization block and did not maintain high spiking activity with a moderate level of current injection (>100 pA), whereas MPOA^{ESR1} cells in mothers continued to increase firing with large current injections (Fig. 6a,b). The excitability of MPOA^{ESR1} cells in maternal virgins was between that of hostile virgins and mothers (Fig. 6a,b). By contrast, the excitability of BNSTpr^{ESR1} cells in hostile and maternal virgin female mice was similar (Fig. 6c,d). However, BNSTpr^{ESR1} cells in mothers were less excitable than those in virgin female mice, as revealed by the spike frequency–current (*F–I*) curves (Fig. 6c,d). Between BNSTpr^{ESR1} and MPOA^{ESR1} cells, MPOA^{ESR1} cells were generally more active, as reflected by their higher maximum action potential number during current injection, and this difference was the largest in mothers (Fig. 6e). Overall, MPOA^{ESR1} cells are more excitable in mothers than in virgin female mice, whereas the opposite is true for BNSTpr^{ESR1} cells. These opposing changes in the excitability of MPOA^{ESR1} and BNSTpr^{ESR1} cells could underlie their reversed in vivo response patterns to pups during motherhood.

Finally, we examined whether the different tendency of SW and C57BL/6 virgin female mice to show infanticidal behaviour could reside in their differences in BNSTpr^{ESR1} cell properties. We recorded BNSTpr^{ESR1} cells from virgin C57BL/6 female mice (BNSTpr$^{ESR1.C57}$) and found that they were much less excitable than those in SW female mice (BNSTpr$^{ESR1.SW}$) (Fig. 6f–i). Approximately half of BNSTpr$^{ESR1.C57}$ cells (23 out of 44) could fire no more than two spikes regardless of the amount of injected current, whereas the same was true for only 1 out of 57 BNSTpr$^{ESR1.SW}$ cells in virgin female mice (Fig. 6f,g). The spiking frequency of BNSTpr$^{ESR1.C57}$ cells was significantly lower than that of BNSTpr$^{ESR1.SW}$ cells in virgin female mice across current steps (Fig. 6h,i). Whereas the excitability of BNSTpr^{ESR1} cells decreased in SW mothers, it did not change in C57BL/6 mothers (Fig. 6h,i). These results revealed dampened excitability of BNSTpr^{ESR1} cells in virgin C57BL/6 female mice that could contribute to a lack of infanticidal behaviours in these animals.

No effect on maternal aggression

We also examined BNSTpr^{ESR1} cell responses and the functional relevance to adult-directed behaviours (Supplementary Note 1). BNSTpr^{ESR1} and BNSTpr^{MPOA} cells in virgin female mice also increased activity during adult-directed social behaviours but to a lesser extent than during infanticide. Importantly, BNSTpr^{ESR1} cells responded minimally during maternal aggression and chemogenetic inactivation of BNSTpr^{ESR1} cells did not alter maternal aggression, supporting a specific role of BNSTpr^{ESR1} cells in pup-directed attack. Optogenetic activation

of BNSTpr^{ESR1} or BNSTpr^{MPOA} cells rarely induced attack towards adults but did increase social grooming and sometimes male-style mounting in virgin female mice. Finally, pathway-specific activation suggested that BNSTpr^{ESR1} optogenetic-activation-induced social grooming was not mediated by its projection to MPOA.

Discussion

Although initially considered to be a rare pathological behaviour, infanticide may in fact be an adaptive behaviour to increase an individual's reproductive success in both male and female animals of many species[12,46]. Here, using MPOA as an entry point, we identified BNSTpr^{ESR1} cells as a key population for driving hostile behaviours towards the young in female mice. Both BNSTpr^{ESR1} and MPOA^{ESR1} cells are primarily GABAergic. They form strong reciprocal inhibition to antagonize each other's behaviour output. During motherhood, the relative activities between BNSTpr^{ESR1} and MPOA^{ESR1} cells reverse to support the substantial behavioural changes of the female mice to ensure the survival of the young (Fig. 6j).

Our study also revealed the infanticide-promoting effect of MeApd^{MPOA} cells. Notably, whereas the BNSTpr is mainly activated by infanticide and the MPOA by maternal care, the MeA is activated by both infanticide and maternal behaviours. The potential dual roles of MeA cells in pup-directed behaviours were also suggested by recent functional studies of MeApd GABAergic cells[27]. Importantly, only FOS induced by infanticide, but not maternal care, preferentially overlaps with MeApd^{MPOA} cells, suggesting that infanticide and maternal care could activate distinct MeApd cells that differ in their projection patterns. Considering that MeApd cells also project strongly to the BNSTpr and the opposing functions of the BNSTpr and MPOA in pup-directed behaviours, it is possible that BNSTpr-projecting and MPOA-projecting MeApd cells mediate different pup-directed behaviours. Future circuit studies will help to test this hypothesis. Notably, the MeA, like the BNSTpr and MPOA, is dominated by GABAergic cells, suggesting that the antagonism between infanticide and maternal circuits probably occurs at multiple levels (Supplementary Note 2).

Note that BNSTpr^{ESR1} is not a homogenous population. A recent study performed a single-cell RNA-sequencing analysis of BNSTpr^{ESR1} cells and identified 36 molecularly distinguishable clusters[47]. It was also previously shown that inhibiting BNSTpr^{ESR1} cells can perturb male aggression and sexual behaviours, although their function in female animals was not tested[48]. It was found that oestrogen-receptor-2-expressing BNST cells, a subpopulation of BNSTpr^{ESR1} cells, mediate sexual satiety in both male and female animals[47,49]. Thus, probably not all BNSTpr^{ESR1} cells mediate infanticide. The molecular identity of infanticide-relevant BNSTpr cells is likely to be refined in future studies (Supplementary Note 2).

A negative circuit that counteracts the maternal circuit has long been suspected[5,6]. Here our study unequivocally demonstrated the existence of an infanticide circuit in female mice and revealed its plasticity over the reproductive state and its variability among individuals with different propensities to kill pups. Our study further uncovered the intimate and antagonistic relationship between infanticide and maternal circuits, highlighting the importance of studying both circuits to understand the generation of infant-directed behaviours under normal and pathological conditions.

Online content

Any methods, additional references, Nature Portfolio reporting summaries, source data, extended data, supplementary information, acknowledgements, peer review information; details of author contributions and competing interests; and statements of data and code availability are available at https://doi.org/10.1038/s41586-023-06147-9.

1. Parmigiani, S. & vom Saal, F. *Infanticide And Parental Care* (Routledge, 2016).
2. Dulac, C., O'Connell, L. A. & Wu, Z. Neural control of maternal and paternal behaviors. *Science* **345**, 765–770 (2014).
3. Soroker, V. & Terkel, J. Changes in incidence of infanticidal and parental responses during the reproductive cycle in male and female wild mice *Mus musculus*. *Anim. Behav.* **36**, 1275–1281 (1988).
4. McCarthy, M. M. & vom Saal, F. S. The influence of reproductive state on infanticide by wild female house mice (*Mus musculus*). *Physiol. Behav.* **35**, 843–849 (1985).
5. Kohl, J., Autry, A. E. & Dulac, C. The neurobiology of parenting: a neural circuit perspective. *Bioessays* **39**, 1–11 (2017).
6. Numan, M. Motivational systems and the neural circuitry of maternal behavior in the rat. *Dev. Psychobiol.* **49**, 12–21 (2007).
7. Kohl, J. & Dulac, C. Neural control of parental behaviors. *Curr. Opin. Neurobiol.* **49**, 116–122 (2018).
8. Yu, Z.-X., Li, X.-Y. & Xu, X.-H. Neural circuit mechanisms that underlie parental care. *Adv. Exp. Med. Biol.* **1284**, 49–62 (2020).
9. Numan, M. & Insel, T. R. *The Neurobiology of Parental Behavior* (Springer, 2003).
10. Kuroda, K. O. & Numan, M. The medial preoptic area and the regulation of parental behavior. *Neurosci. Bull.* **30**, 863–865 (2014).
11. Carollo, A., Balagtas, J. P. M., Neoh, M. J. & Esposito, G. A scientometric approach to review the role of the medial preoptic area (MPOA) in parental behavior. *Brain Sci.* **11**, 393 (2021).
12. Lukas, D. & Huchard, E. The evolution of infanticide by females in mammals. *Philos. Trans. R. Soc. B* **374**, 20180075 (2019).
13. Palombit, R. A. Infanticide as sexual conflict: coevolution of male strategies and female counterstrategies. *Cold Spring Harb. Perspect. Biol.* **7**, a017640 (2015).
14. Jakubowski, M. & Terkel, J. Infanticide and caretaking in non-lactating *Mus musculus*: influence of genotype, family group and sex. *Anim. Behav.* **30**, 1029–1035 (1982).
15. Svare, B. & Mann, M. Infanticide: genetic, developmental and hormonal influences in mice. *Physiol. Behav.* **27**, 921–927 (1981).
16. Gandelman, R. The ontogeny of maternal responsiveness in female Rockland-Swiss albino mice. *Horm. Behav.* **4**, 257–268 (1973).
17. Wei, Y. C. et al. Medial preoptic area in mice is capable of mediating sexually dimorphic behaviors regardless of gender. *Nat. Commun.* **9**, 279 (2018).
18. Fang, Y. Y., Yamaguchi, T., Song, S. C., Tritsch, N. X. & Lin, D. A hypothalamic midbrain pathway essential for driving maternal behaviors. *Neuron* **98**, 192–207 (2018).
19. Wu, Z., Autry, A. E., Bergan, J. F., Watabe-Uchida, M. & Dulac, C. G. Galanin neurons in the medial preoptic area govern parental behaviour. *Nature* **509**, 325–330 (2014).
20. Kohl, J. et al. Functional circuit architecture underlying parental behaviour. *Nature* **556**, 326–331 (2018).
21. Tsuneoka, Y. et al. Neurotransmitters and neuropeptides in gonadal steroid receptor-expressing cells in medial preoptic area subregions of the male mouse. *Sci. Rep.* **7**, 9809 (2017).
22. Li, X. Y. et al. AGRP neurons project to the medial preoptic area and modulate maternal nest-building. *J. Neurosci.* **39**, 456–471 (2019).
23. Zhang, G.-W. et al. Medial preoptic area antagonistically mediates stress-induced anxiety and parental behavior. *Nat. Neurosci.* **24**, 516–528 (2021).
24. Tsuneoka, Y. et al. Distinct preoptic-BST nuclei dissociate paternal and infanticidal behavior in mice. *EMBO J.* **34**, 2652–2670 (2015).
25. Autry, A. E. et al. Urocortin-3 neurons in the mouse perifornical area promote infant-directed neglect and aggression. *eLife* **10**, e64680 (2021).
26. Sato, K. et al. Amygdalohippocampal area neurons that project to the preoptic area mediate infant-directed attack in male mice. *J. Neurosci.* **40**, 3981–3994 (2020).
27. Chen, P. B. et al. Sexually dimorphic control of parenting behavior by the medial amygdala. *Cell* **176**, 1206–1221 (2019).
28. Numan, M. Medial preoptic area and maternal behavior in the female rat. *J. Compar. Physiol. Psychol.* **87**, 746–759 (1974).
29. Numan, M., Corodimas, K. P., Numan, M. J., Factor, E. M. & Piers, W. D. Axon-sparing lesions of the preoptic region and substantia innominata disrupt maternal behavior in rats. *Behav. Neurosci.* **102**, 381–396 (1988).
30. Mann, M. A., Kinsley, C., Broida, J. & Svare, B. Infanticide exhibited by female mice: genetic, developmental and hormonal influences. *Physiol. Behav.* **30**, 697–702 (1983).
31. Zingg, B. et al. AAV-mediated anterograde transsynaptic tagging: mapping corticocollicular input-defined neural pathways for defense behaviors. *Neuron* **93**, 33–47 (2017).
32. Madisen, L. et al. A robust and high-throughput Cre reporting and characterization system for the whole mouse brain. *Nat. Neurosci.* **13**, 133–140 (2010).
33. Chen, A.-X. et al. Specific hypothalamic neurons required for sensing conspecific male cues relevant to inter-male aggression. *Neuron* **108**, 763–774 (2020).
34. Stagkourakis, S. et al. A neural network for intermale aggression to establish social hierarchy. *Nat. Neurosci.* **21**, 834–842 (2018).
35. Gallo, M. et al. Limited bedding and nesting induces maternal behavior resembling both hypervigilance and abuse. *Front. Behav. Neurosci.* **13**, 167 (2019).
36. Nephew, B. C. & Bridges, R. S. Effects of chronic social stress during lactation on maternal behavior and growth in rats. *Stress* **14**, 677–684 (2011).
37. Kim, S. Y. et al. Diverging neural pathways assemble a behavioural state from separable features in anxiety. *Nature* **496**, 219–223 (2013).
38. Jennings, J. H. et al. Distinct extended amygdala circuits for divergent motivational states. *Nature* **496**, 224–228 (2013).
39. Lebow, M. A. & Chen, A. Overshadowed by the amygdala: the bed nucleus of the stria terminalis emerges as key to psychiatric disorders. *Mol. Psychiatry* **21**, 450–463 (2016).
40. Mitra, S. W. et al. Immunolocalization of estrogen receptor β in the mouse brain: comparison with estrogen receptor α. *Endocrinology* **144**, 2055–2067 (2003).
41. Lee, H. et al. Scalable control of mounting and attack by Esr1^{+} neurons in the ventromedial hypothalamus. *Nature* **509**, 627–632 (2014).
42. Hashikawa, K. et al. Esr1^{+} cells in the ventromedial hypothalamus control female aggression. *Nat. Neurosci.* **20**, 1580–1590 (2017).

43. Yamaguchi, T. et al. Posterior amygdala regulates sexual and aggressive behaviors in male mice. *Nat. Neurosci.* **23**, 1111–1124 (2020).
44. Kelly, D. A., Varnum, M. M., Krentzel, A. A., Krug, S. & Forger, N. G. Differential control of sex differences in estrogen receptor α in the bed nucleus of the stria terminalis and anteroventral periventricular nucleus. *Endocrinology* **154**, 3836–3846 (2013).
45. Nguyen, A. Q., Dela Cruz, J. A., Sun, Y., Holmes, T. C. & Xu, X. Genetic cell targeting uncovers specific neuronal types and distinct subregions in the bed nucleus of the stria terminalis. *J. Comp. Neurol.* **524**, 2379–2399 (2016).
46. Hrdy, S. B. Infanticide among animals: a review, classification, and examination of the implications for the reproductive strategies of females. *Ethol. Sociobiol.* **1**, 13–40 (1979).
47. Knoedler, J. R. et al. A functional cellular framework for sex and estrous cycle-dependent gene expression and behavior. *Cell* **185**, 654–671 (2022).
48. Yang, B., Karigo, T. & Anderson, D. J. Transformations of neural representations in a social behaviour network. *Nature* **608**, 741–749 (2022).
49. Zhou, X. et al. Hyperexcited limbic neurons represent sexual satiety and reduce mating motivation. *Science* **379**, 820–825 (2023).

Methods

Mice

All procedures were approved by the NYULMC Institutional Animal Care and Use Committee (IACUC) in compliance with the US National Institutes of Health (NIH) Guidelines for the Care and Use of Laboratory Animals. Adult male mice (aged 8–16 weeks) were used as test subjects for all studies. Mice were housed under a 12 h–12 h light–dark cycle (dark cycle, 10:00 to 22:00), with food and water available ad libitum. Room temperature was maintained between 20–22 °C and humidity between 30–70%, with a daily average approximately 45%. Esr1-2A-cre mice were provided initially by the D. J. Anderson laboratory (Caltech) and are currently available from Jackson Laboratory (017911). Esr1-2A-cre mice of the SW background were backcrossed with SW wild-type mice for at least five generations. All experimental Esr1-2A-cre mice are heterozygous. Ai6 mice were purchased from the Jackson Laboratory (007906) and were backcrossed to either SW or C57BL/6 for at least five generations. Wild-type SW mice were purchased from Taconic. Wild-type C57BL/6 and BALB/c mice were purchased from Charles River, postnatal day 1–5 (P1–5) pups used for behavioural experiments were bred in-house. Mice were housed under a 12 h–12 h light–dark cycle (22:00–10:00 light), with food and water available ad libitum. All mice were group housed until adulthood. After surgery, mice were single housed unless they were paired with a male and, after they became pregnant, they were single housed again until having a litter. Animals were randomly assigned to test and control groups.

Virus

AAV2-CAG-Flex-GCaMP6f was purchased from the University of Pennsylvania vector core. AAV2-hSyn-FLEX-GFP, AAV2-hSyn-Flex-ArchT-TdTomato, AAV2-hSyn-Flex-ChrimsonR-tdTomato and AAV2-EF1a-DIO-ChR2-eYFP were purchased from the University of North Carolina vector core. AAV1-hSyn-cre, AAV2-hSyn-DIO-mCherry, AAV2-hSyn-DIO-hM3Dq-mCherry and AAV2-hSyn-DIO-hM4Di-mCherry were purchased from Addgene. AAV8-hSyn-DIO-DTR was purchased from Boston Children's Hospital. The titre of AAV1-hSyn-cre was higher than 2×10^{13} genomic copies per ml. The titre of other viruses ranged from 2×10^{12} to 2×10^{13} genomic copies per ml.

Stereotactic surgery

Mice (aged 8–20 weeks old) were anaesthetized with 1–2% isoflurane and positioned on a stereotaxic rig (Kopf Instruments, Model 1900). Viruses were delivered into the brains through a glass capillary using a nanoinjector (World Precision Instruments, Nanoliter 2000).

To investigate infanticide-induced FOS expression in MPOA-connected cells, 50 nl AAV1-hSyn-cre (titre $>2 \times 10^{13}$) and 50 nl AAV2-hSyn-DIO-mCherry were mixed and injected into unilateral MPOA (anteroposterior (AP): 0 mm, mediolateral (ML): −0.3 mm, dorsoventral (DV): −4.95 mm; coordinates are shown relative to bregma) of SW Ai6 female mice.

To ablate MPOA^{ESR1} cells, 300 nl AAV8-hSyn-DIO-DTR (control: AAV2-hSyn-DIO-mCherry) was injected bilaterally into the MPOA (AP: 0 mm, ML: ±0.3 mm, DV: −4.95 mm) of heterozygous virgin Esr1-2A-cre female mice in the SW background. To chemogenetically inhibit MPOA^{ESR1} cells, 300 nl AAV2-hSyn-DIO-hM4Di-mCherry (control: AAV2-hSyn-DIO-mCherry) was injected bilaterally into the MPOA (AP: 0 mm, ML: ±0.3 mm, DV: −4.95 mm) of heterozygous virgin Esr1-2A-cre female mice in the SW background. All female mice were screened before surgery, and only female mice that did not show spontaneous infanticide were used.

To chemogenetically activate MPOA-connecting cells in various brain regions, we injected a 200 nl 1:1 mixture of AAV1-hSyn-cre (titre $>2 \times 10^{13}$) and AAV2-hSyn-Flex-GFP bilaterally into the MPOA (AP: 0 mm, ML: ±0.3 mm, DV: −4.95 mm) and, at the same time, AAV2-hSyn-DIO-hM3Dq-mCherry bilaterally into the BNSTpr (AP: −0.45 mm, ML: ±0.9 mm, DV: −3.6 mm; 300 nl per side), MeApd (AP: −2.0 mm, ML: ±2.25 mm, DV: −4.6 mm; 200 nl per side), PVT (AP: −0.96 mm, ML: ±0.2 mm, DV: −3.17 mm; 100 nl per side), PVN (AP: −0.6 mm, ML: ±0.3 mm, DV: −4.3 mm; 100 nl per side), VMHvl (AP: −1.8 mm, ML: ±0.75 mm, DV: −5.6 mm; 50 nl per side), PMv (AP: −2.35 mm, ML: ±0.5 mm, DV: −5.6 mm; 200 nl per side) or SUM (AP: −3.06 mm, ML: ±0.4 mm, DV: −4.7 mm; 100 nl per side). For control female mice, AAV2-hSyn-DIO-mCherry was injected into the target region.

To chemogenetically inhibit BNSTpr^{ESR1} neurons, we injected AAV2-hSyn-DIO-hM4Di-mCherry (control: AAV2-hSyn-DIO-mCherry) bilaterally into the BNSTpr (AP: −0.45 mm, ML: ±0.9 mm, DV: −3.6 mm; 300 nl per side) of adult virgin Esr1-2A-cre female mice in the SW background.

To optogenetically activate BNSTpr^{MPOA} neurons, we injected 200 nl 1:1 mixture of AAV1-hSyn-cre (titre, $>2 \times 10^{13}$) and AAV2-hSyn-Flex-GFP bilaterally into the MPOA (AP: 0 mm, ML: ±0.3 mm, DV: −4.95 mm) and, at the same time, AAV2-EF1a-DIO-ChR2-eYFP bilaterally into the BNSTpr (AP: −0.45 mm, ML: ±0.9 mm, DV: −3.6 mm; 300 nl per side) of adult C57BL/6 female mice. To optogenetically activate BNSTpr^{ESR1} neurons, we injected AAV2-EF1a-DIO-ChR2-eYFP bilaterally into the BNSTpr (AP: −0.45 mm, ML: ±0.9 mm, DV: −3.6 mm; 300 nl per side) of adult virgin Esr1-2A-cre female mice of the C57BL/6 and SW background. During the surgery and after virus injection, two 200 μm optical fibres (Thorlabs, FT200EMT, CFLC230) were inserted 500 μm above the virus injection sites, one into each side, and secured on the skull using adhesive dental cement (C&B Metabond, S380). SW adult female mice were screened before surgery to ensure no spontaneous infanticide.

To optogenetically inactivate BNSTpr^{ESR1} projection to MPOA, we injected AAV2-hSyn-Flex-ArchT-TdTomato (control: AAV2-hSyn-DIO-mCherry) bilaterally into the BNSTpr (AP: −0.45 mm, ML: ±0.9 mm, DV: −3.6 mm; 300 nl per side) of Esr1-2A-cre female mice in the SW background. During the same surgery, two 400 μm optical fibres (Doric, DFC_400/430) were inserted 500 μm above the MPOA (AP: 0 mm, ML: ±0.3 mm, DV: −4.45 mm), one on each side, and secured onto the skull using adhesive dental cement (C&B Metabond, S380). All female mice were screened before surgery, and only female mice that showed spontaneous infanticide were used.

To optogenetically inactivate MPOA^{ESR1} projection to the BNSTpr, we injected AAV2-hSyn-Flex-ArchT-TdTomato (control: AAV2-hSyn-DIO-mCherry) bilaterally into the MPOA (AP: 0 mm, ML: ±0.3 mm, DV: −4.95 mm; 300 nl per side) of Esr1-2A-cre female mice in the SW background. During the surgery and after virus injection, two 200 μm optical fibres (Thorlabs, FT200EMT, CFLC230) were inserted 500 μm above the BNSTpr (AP: −0.45 mm, ML: ±0.9 mm, DV: −3.1 mm), one on each side, and secured onto the skull using adhesive dental cement (C&B Metabond, S380). All female mice were screened before surgery, and only female mice that did not show spontaneous infanticide were used.

To optogenetically activate BNSTpr^{ESR1} projection to MPOA, we injected AAV2-hSyn-Flex-ChrimsonR-tdTomato (group 1) or AAV2-EF1a-DIO-ChR2-eYFP mixed with AAV2-hSyn-DIO-hM4Di-mCherry (group 2) bilaterally into the BNSTpr (AP: −0.45 mm, ML: ±0.9 mm, DV: −3.6 mm; 300 nl per side for group 1, 500 nl per side for group 2). During the surgery and after virus injection, two 400 μm optical fibres (Doric, DFC_400/430) were inserted 500 μm above the MPOA (AP: 0 mm, ML: ±0.3 mm, DV: −4.45 mm), one on each side, and secured onto the skull using adhesive dental cement (C&B Metabond, S380). Control female mice were injected with AAV2-hSyn-DIO-mCherry. Control and group 1 female mice were screened before surgery, and only female mice that did not show spontaneous infanticide were used. Group 2 female mice were screened before surgery, and only female mice that showed spontaneous pup retrieval were used.

To optogenetically activate MPOA^{ESR1} projection to the BNSTpr, we injected AAV2-hSyn-Flex-ChrimsonR-tdTomato (group 1) or AAV2-EF1a-DIO-ChR2-eYFP mixed with AAV2-hSyn-DIO-hM4Di-mCherry

(group 2) bilaterally into the MPOA (AP: 0 mm, ML: ±0.3 mm, DV: −4.95 mm; 300 nl per side for group 1, 500 nl per side for group 2). During the surgery and after virus injection, two 200 μm optical fibres (Thorlabs, FT200EMT, CFLC230) were inserted 500 μm above the BNSTpr (AP: −0.45 mm, ML: ±0.9 mm, DV: −3.1 mm), one on each side, and secured onto the skull using adhesive dental cement (C&B Metabond, S380). Control female mice were injected with AAV2-hSyn-DIO-mCherry. All female mice were screened before surgery, and only infanticidal female mice were used.

To record the Ca^{2+} signal of $MPOA^{ESR1}$ or $BNSTpr^{ESR1}$ cells, 300 nl AAV2-CAG-Flex-GCaMP6f (control: AAV2-hSyn-Flex-GFP) was injected unilaterally into the MPOA (AP: 0 mm, ML: −0.3 mm, DV: −4.95 mm) or the BNSTpr (AP: −0.45 mm, ML: −0.9 mm, DV: −3.6 mm) of heterozygous virgin Esr1-2A-cre female mice in the SW background. To record Ca^{2+} signals of $BNSTpr^{MPOA}$ cells, 100 nl AAV1-hSyn-cre (titre $>2 \times 10^{13}$) and 100 nl AAV2-hSyn-DIO-mCherry were mixed and injected unilaterally into the MPOA (AP: 0 mm, ML: −0.3 mm, DV: −4.95 mm) and, at the same time, 300 nl AAV2-CAG-Flex-GCaMP6f was injected unilaterally into the BNSTpr (AP: −0.45 mm, ML: −0.9 mm, DV: −3.6 mm) of WT virgin SW female mice. After virus injection, a 400 μm optical fibre assembly (Thorlabs, FR400URT, CF440) was inserted 300 μm above the virus injection site and secured onto the skull using adhesive dental cement (C&B Metabond, S380). Recording started at least 3 weeks after surgery.

To simultaneously record the Ca^{2+} signal of $MPOA^{ESR1}$ or $BNSTpr^{ESR1}$ cells, 300 nl AAV2-CAG-Flex-GCaMP6f was injected unilaterally into the MPOA (AP: 0 mm, ML: −0.3 mm, DV: −4.95 mm) and contralaterally into the BNSTpr (AP: −0.45 mm, ML: +0.9 mm, DV: −3.6 mm) of heterozygous virgin Esr1-2A-cre female mice in the SW background. After the virus injection, an optical fibre assembly containing two 100 μm optic fibres (USCONEC, C12405, Ferrule_48F) was secured onto the skull using adhesive dental cement (C&B Metabond, S380). The optic fibres ended 50 μm above the virus injection sites. Recording started at least 4 weeks after surgery.

For anterograde tracing of $BNSTpr^{ESR1}$ and $MPOA^{ESR1}$ neurons, 50 nl AAV2-hSyn-FLEX-GFP was injected unilaterally into the BNSTpr (AP: −0.45 mm, ML: −0.9 mm, DV: −3.6 mm) or MPOA (AP: 0 mm, ML: −0.3 mm, DV: −4.95 mm) of virgin Esr1-2A-cre female mice with the SW background.

To examine the synaptic connection from $BNSTpr^{ESR1}$ cells to $MPOA^{ESR1}$ cells using slice electrophysiology, we injected AAV2-EF1a-DIO-ChR2-eYFP bilaterally into the BNSTpr (AP: −0.45 mm, ML: ±0.9 mm, DV: −3.6 mm; 300 nl per side), and at the same time injected AAV2-hSyn-DIO-mCherry bilaterally into the MPOA (AP: 0 mm, ML: ±0.3 mm, DV: −4.95 mm; 300 nl per side). To examine $MPOA^{ESR1}$ to $BNSTpr^{ESR1}$ projection, we injected AAV2-EF1a-DIO-ChR2-eYFP bilaterally into the MPOA (AP: 0 mm, ML: ±0.3 mm, DV: −4.95 mm; 300 nl per side), and at the same time AAV2-hSyn-DIO-mCherry bilaterally into the BNSTpr (AP: −0.45 mm, ML: ±0.9 mm, DV: −3.6 mm; 300 nl per side). All mice were heterozygous virgin Esr1-2A-cre female mice of the SW background.

To examine the intrinsic properties of $MPOA^{ESR1}$ and $BNSTpr^{ESR1}$ cells, we injected AAV2-hSyn-FLEX-GFP bilaterally into the MPOA (AP: 0 mm, ML: ±0.3 mm, DV: −4.95 mm; 300 nl per side) and BNSTpr (AP: −0.45 mm, ML: ±0.9 mm, DV: −3.6 mm; 300 nl per side) in each animal. All mice were heterozygous virgin Esr1-2A-cre female mice of the SW or C57BL/6 background.

To validate ArchT-mediated terminal inactivation for $MPOA^{ESR1}$–BNSTpr pathway, we injected a mixture of 150 nl AAV2-hSyn-Flex-ArchT-TdTomato and 150 nl AAV2-EF1a-DIO-ChR2-eYFP bilaterally into the MPOA (AP: 0 mm, ML: −0.3 mm, DV: −4.95 mm) and, at the same time, 200 nl AAV2-CAG-Flex-GCaMP6f bilaterally into the BNSTpr (AP: −0.45 mm, ML: +0.9 mm, DV: −3.6 mm) of SW virgin Esr1-2A-cre female mice. To validate ArchT-mediated terminal inactivation for $BNSTpr^{ESR1}$–MPOA projection, we injected a mixture of 150 nl AAV2-hSyn-Flex-ArchT-TdTomato and 150 nl AAV2-EF1a-DIO-ChR2-eYFP bilaterally into the BNSTpr (AP: −0.45 mm, ML: +0.9 mm, DV: −3.6 mm), and 200 nl AAV2-CAG-Flex-GCaMP6f bilaterally into the MPOA (AP: 0 mm, ML: −0.3 mm, DV: −4.95 mm) of SW Esr1-2A-cre female mice.

$MPOA^{ESR1}$ cell ablation

SW female mice were prescreened, and only non-infanticide female mice were used for surgery. During the screening, two pups were introduced into the home cage of the test female mouse for 10 min. Then, 3 weeks after surgery, we tested the behaviours towards the pups on the day before diphtheria toxin injection. During the test, two P1–5 pups were introduced into the home cage of the test female mouse at a location distant from the nest for 10 min. After the test, we injected diphtheria toxin (50 μg per kg, 5 μg per ml dissolved in PBS) intraperitoneally into each female mouse. Then, 7 days later, female mice were tested again by introducing two P1–5 pups into the test female's home cage at a location distant from the nest, wounded pups were euthanized and the test was stopped if the female mice attacked them and caused physical damage in the 10 min testing period.

Pharmacogenetic activation and inactivation

For pharmacogenetic inhibition of $MPOA^{ESR1}$ cells, SW female mice were screened before the surgery by introducing two pups into the home cage of the female mouse for 10 min. Only female mice that did not attack pups during the screening were used for surgery. Then, 3 weeks after virus injection, sterile saline or CNO (1 mg per kg) was injected intraperitoneally 30 min before behavioural assays on separate days. Saline was always injected the day before CNO injection. During the test, two P1–5 pups were introduced into the home cage of the test female mouse at a location distant from the nest for 10 min. If the tested female mice attacked and caused physical damage to pups in the 10 min testing period, the test was stopped, and the wounded pups were immediately euthanized.

For pharmacogenetic activation of MPOA-connecting cells in the BNSTpr, MeApd, PVT, PVN, VMHvl, PMv and SUM, female mice were not screened as infanticide is very rare in C57BL/6 female mice. Then, 3 weeks after virus injection, sterile saline or CNO (1 mg per kg) was injected intraperitoneally 30 min before behavioural assays on separate days. Saline was always injected the day before CNO injection. During the 10 min behaviour test, three P1–5 pups were introduced into the home cage of the test female mouse for 10 min at a location distant from the nest. We euthanized the pups immediately after the test if they were attacked by the female mice.

For pharmacogenetic inhibition of $BNSTpr^{ESR1}$ neurons assay, 16 hM4Di and 16 mCherry control female mice were tested in the virgin state. Among them, 9 hM4Di and 8 mCherry virgin female mice showed spontaneous infanticide, and they constitute the infanticide group shown in Fig. 2q; 6 hM4Di and 5 mCherry virgin female mice ignored pups, and they constitute the non-infanticidal animals shown in Extended Data Fig. 8b. Then, 3 weeks after surgery, we injected saline and, 1 day later, CNO (1 mg per kg). Then, 30 min after injection, we introduced 3–4 pups into the home cage of the female mouse for 10 min if no attack occurred. If the tested female mice attacked and caused physical damage to pups in the 10 min testing period, the test was stopped, and the wounded pups were immediately euthanized. After completing the test under a virgin state, each female mouse was paired with a male mouse until they became visibly pregnant. A total of 11 hM4Di and 9 mCherry female mice became mothers. All 11 hM4Di and 8 mCherry lactating female mice showed maternal aggression. For the pup interaction test in lactating female mice (postpartum days 3 and 4), we removed all pups from the cage and injected either saline or CNO on separate days. Then, 30 min after drug injection, 5 pups were introduced into the home cage of the test female mouse for 10 min. Afterwards, we removed all of the pups, and introduced an adult group-housed BALB/c female mouse into the test female's home

cage for 10 min followed by an adult BALB/c male mouse for 10 min with 10 min in between.

Optogenetic activation

For $BNSTpr^{MPOA}$ optogenetic activation, 11 and 8 WT C57BL/6 virgin adult female mice were injected with ChR2 and GFP viruses, respectively. For $BNSTpr^{ESR1}$ optogenetic activation, 8 C57BL/6 and 5 SW Esr1-2A-cre virgin female mice were injected with ChR2 virus, and 8 C57BL/6 virgin Esr1-2A-cre female mice were injected with GFP virus. For ChR2 mice, after testing in the virgin state, each was paired with a male. A total of 6 C57BL/6 female mice and 4 SW Esr1-2A-cre female mice became mothers and were tested again during lactation. Esr1-2A-cre SW female mice were screened before the surgery, and only female mice that did not show infanticide were used.

Three weeks after surgery, the implanted optic fibre assembly was coupled to a patch cord using a zirconia split sleeve (Thorlab, ADAL1-5) to deliver 473 nm laser pulses to the brain. The laser pulses were controlled by TTL signals generated using an RP2 processor (TDT). Regardless of the intruder type, for each test session, 9 sham stimulation trials (0 mW, 20 s) were first delivered, followed by 9 light stimulation trials at each laser intensity (20 ms, 20 Hz, 20 s, 0.5, 1, 2, 3, 4 and 5 mW). The intertrial interval was approximately 60 s, although it could be longer sometimes due to replacing wounded pups. For testing pup-directed behaviours in virgins, we introduced 3–4 P1–5 pups at the beginning of a session. When testing in lactating female mice, all pups of the dam were removed 10 min before the test session and reintroduced right before the session started. If a pup was attacked, we replaced it with a new one and euthanized the wounded pup. For adult female and male sessions, an adult group housed BALB/c female, then a BALB/c male was introduced, and sham and light stimulation were delivered using the same stimulation protocol during the pup interaction test. The first pulse train started for both sham and stimulation trials at a given laser intensity when the testing female investigated the intruder.

For the RTPP test, sham then 20 ms, 20 Hz, 3 mW light pulses were delivered whenever the animal entered the predesignated stimulation chamber and terminated when the animal moved out of the chamber. Each test lasted for 10 min. For the EPM test, mice were habituated to the test area for 2 days, 20 min a day. During the test, we delivered no light for the first 20 min, then 3 mW light pulses for 20 min. The body centre of the animal was tracked using DeepLabCut[50] and was used to calculate the time the animal spent in each chamber in the RTPP test and in the open/closed arms in the EPM test.

Optogenetic terminal activation and inhibition

For $BNSTpr^{ESR1}$–MPOA terminal inhibition, we prescreened SW Esr1-2A-cre virgin female mice before the surgery and used only female mice that showed spontaneous infanticide for surgery. For $MPOA^{ESR1}$–BNSTpr terminal inhibition, we used only SW Esr1-2A-cre virgin female mice that did not show spontaneous infanticide for surgery. Then, 4 weeks after virus injection, we introduced two P1–5 pups into the home cage of the female mouse, far from the nest, for 10 min if no attack occurred. If the tested female mice attacked and caused physical damage to the pups during the 10 min testing period, the test was stopped, and the wounded pups were immediately euthanized. During the pup interaction test, we continuously delivered either sham (0 mW) or 5 mW 589 nm light (Shanghai Dream Laser). The sham stimulation session occurred on the day before the light stimulation session. If the female mouse attacked a pup, we euthanized the pup after the test.

For $BNSTpr^{ESR1}$–MPOA terminal activation (without $BNSTpr^{ESR1}$ inhibition), we only used female mice that did not show spontaneous infanticide during the presurgery pup interaction test. For $MPOA^{ESR1}$–BNSTpr activation (without $MPOA^{ESR1}$ inhibition), we used only female mice that showed spontaneous infanticide before surgery. Then, 4 weeks after the surgery, we introduced two pups into the home cage of the female mouse for 10 min if no attack occurred. If the tested female mice attacked and caused physical damage to pups during the 10 min testing period, the test was stopped, and wounded pups were immediately euthanized. We delivered either sham (0 mW) or 5 mW 20 ms 20 Hz 589 nm light pulses during the entire session. The sham stimulation session occurred on the day before the light situation session.

For $BNSTpr^{ESR1}$–MPOA terminal activation and simultaneous $BNSTpr^{ESR1}$ inhibition, we used only female mice that showed spontaneous retrieval before surgery. For $MPOA^{ESR1}$–BNSTpr terminal activation and simultaneous $MPOA^{ESR1}$ inhibition, we used only spontaneous infanticidal female mice. Then, 4 weeks after surgery and on the day of testing, we i.p. injected CNO (1 mg per kg) and, 30 min later, introduced 2 pups (P1–5) into the home cage of the female mouse and delivered sham (0 mW) or 20 ms 20 Hz 473 nm light for 10 min. If a pup was attacked by the female mouse, it was euthanized after the test.

After the pup interaction test, for $BNSTpr^{ESR1}$–MPOA (both with and without $BNSTpr^{ESR1}$ inhibition) animals, an adult group-housed BALB/c female mouse and then a BALB/c male mouse was introduced, and the same light stimulation protocol was applied.

After completing the behaviour experiments and on a separate day, we delivered 5 mW 20 ms 20 Hz 589 nm light pulses for 10 min to one side of the MPOA or BNSTpr of ChrimsonR animals. We i.p. injected CNO (1 mg per kg) to ChR2 + G_i animals and then, 30 min later, delivered 5 mW 20 ms 20 Hz 473 nm light pulses to one side of the MPOA or BNSTpr for 10 min. Next, 90 min after the light delivery, we perfused the animal and collected the brain for FOS staining.

Behavioural analyses

Animal behaviours were recorded from both the top and side using two synchronized cameras (Edmund, 89533) controlled by StreamPix (NORPIX) at 25 fps. Behaviours were manually annotated frame-by-frame using custom software written in MATLAB (https://pdollar.github.io/toolbox/). 'Approach pup' is when the testing female faces and walks straight to the pup. 'Investigate pup' is when the female's nose closely contacts any body parts of a pup. 'Attack pup' is defined as biting a pup and is confirmed by the wounds. 'Retrieve pup' is defined as the moment the female lifts the pup using its jaw to the moment the pup is dropped in or around the nest. 'Groom pup' is defined as close interaction between the female and pup accompanied by rhythmic up and down head movement of the female and displacement of the pup. 'Investigate female/male' is defined as nose-to-face, nose-to-trunk or nose-to-urogenital contact. 'Social groom' is defined as licking or grooming the head or neck area of the adult intruder. 'Mount' is when the testing female mouse clasps onto the flank of the adult intruder, establishes an on-top position, and moves its pelvis rhythmically. 'Attack female/male' is defined as lunging, biting and fast movements connecting these behaviours. During annotation, the experimenter was not blinded to the treatment (e.g., ChR2, GCaMP6 or mCherry group) but was blinded to the neural responses of the subject animal.

Determination of the oestrous state

We washed the vaginal area of the female mouse using 50 µl saline several times, mounted the washed solution on a slide and examined the cell morphology under a light microscope to determine the oestrous state of the female mice. If the vaginal cytology showed the presence of mainly cornified epithelial cells, the female mouse was determined to be in the oestrus state; if leukocytes were the main cell type in vaginal cytology, the female mouse was determined to be in the dioestrus state.

Fibre photometry

For single-region fibre photometry recording, the fluorescence signals were performed as described previously[18,43]. In brief, 390 Hz sinusoidal blue LED light (30 µW; LED light: M470F1; LED driver: LEDD1B; Thorlabs) was band-pass filtered (passing band: 472 ± 15 nm, FF02-472/30-25, Semrock) and delivered to the brain to excite GCaMP6f. The emission light travelled back through the same optic fibre and was band-pass

filtered (passing bands: 535 ± 25 nm, FF01-535/505, Semrock), passed through an adjustable zooming lens (Thorlab, SM1NR01 and Edmund optics, 62-561), detected by a Femtowatt Silicon Photoreceiver (Newport, 2151) and recorded using a real-time processor (RP2, TDT). The envelope of the 390 Hz signals reflected the intensity of the GCaMP and was extracted in real-time using a custom TDT program. The signal was low-pass filtered with a cut-off frequency of 10 Hz. The blue LED was adjusted so that the light intensity at the tip of the optical fibre was 30 μW. The baseline fluorescence was set around 1 AU for all animals by adjusting the zooming lens attached to the photoreceiver.

For fibre photometry recording of $MPOA^{ESR1}$ neurons, 11 female mice were injected with AAV2-CAG-Flex-GCaMP6f. A total of 5 out of 11 female mice showed infanticide 3 weeks after surgery, and were used for recording. For virgin female mice, all recordings were performed in dioestrus mice, which was determined on the basis of vaginal cytology. During the first recording session, animals were left alone in their home cage for around 10 min, and then a P1–5 pup was introduced at a location distant from the nest. After naturally occurring infanticide, the pup was removed and euthanized. A total of 3–5 pups was introduced during the recording session, each for approximately 1–2 min. After the recording session with the pups, we introduced a group-housed adult BALB/c female mouse and then an adult BALB/c male mouse into the cage of the recording female mouse, each for 10 min with 10 min in between. After recording in a hostile virgin state, female mice were exposed to pups for more than 30 min each day for 1–2 weeks. During the first 3–7 days of pup sensitization, pups were presented under a cup to prevent infanticide. Once female mice stopped infanticide, they were allowed to freely interact with 3–5 pups for another 2–7 days until they quickly retrieved all pups back to nest on two consecutive days. We then performed fibre photometry recordings again. During the recording, 3–5 pups were introduced into the cage of the female mouse far from the nest for approximately 10 min. Next, adult male and female intruders were introduced sequentially in the same way as the recording under the hostile virgin state. After completing both recording sessions, we paired each female mouse with an adult male mouse until the female mouse became visibly pregnant. On postpartum day 2 or 3, mothers were recorded with the same procedure as in the maternal virgin state.

For fibre photometry recording of $BNSTpr^{ESR1}$ neurons, 14 female mice that were injected with AAV2-CAG-Flex-GCaMP6f showed the proper virus expression and fibre placement. A total of 8 out of 14 female mice showed infanticide, and 7 out of 8 female mice became mothers. So, 7 female mice were recorded from virgin to lactating state. For fibre photometry recording of $BNSTpr^{MPOA}$ neurons, 6 female mice were recorded from virgin to lactating state. The recording procedure was the same as for recording $MPOA^{ESR1}$ cells in hostile virgin female mice and mothers. Control GFP animals underwent the same recording protocol.

For simultaneous recording of $MPOA^{ESR1}$ and $BNSTpr^{ESR1}$ neurons, we injected viruses into six female mice. A total of 3 out of 6 female mice had correct virus expression and fibre placements in both regions, showed infanticide in the virgin state and became mothers. The multifibre recording setup was the same as described in our previous study[51]. In brief, blue LED light (Thorlabs, M470F1, LEDD1B) was band-pass filtered (Semrock, FF02-472/30-25), reflected onto a dichroic filter (Semrock, FF495-Di03-25x36) and coupled into a custom designed 100 μm fibre bundle (Doric Lenses) through an Olympus PLN ×10 objective (Edmunds, 86-813). Emission light was band-pass filtered (Semrock, FF01-535/50) and projected onto the CCD sensor of a camera (Basler, acA640-120gc) through an achromatic doublet (Thorlabs, AC254-060-A-ML). The LED was driven by DC current, and the light intensity at the tip of the fibre was set to be ~30 μW. The sampling rate of the camera was 25 fps. After video acquisition, we calculated the average pixel value at each fibre end as the raw fluorescence signal (F_{raw}).

During the recording in the virgin state, after recording the baseline activity for 10 min, one pup was introduced into the recording female home cage and, after naturally occurring infanticide, we removed and euthanized the pup and introduced a new pup into the cage. Up to 5 pups were introduced during each recording session, which lasted approximately 15 min. During the recording in the lactating state, all pups were taken out and then introduced into the cage one by one over 15 min.

To analyse the recording data, the MATLAB function msbackadj with a moving window of 25% of the total recording duration was first applied to the raw Ca^{2+} signal F_{raw} to get the flatted signal F_{flat}. Then the instantaneous baseline signal was obtained as $F_{baseline} = F_{raw} - F_{flat}$. The $\Delta F/F$ was then calculated as $\Delta F/F = (F_{raw} - F_{baseline})/F_{baseline}$. The Z-scored ΔF/F was then calculated as $Z = (x - \mu)/\sigma$ (where μ is the mean of $\Delta F/F$ and σ is the s.d. of $\Delta F/F$). The PETHs were constructed by aligning the Z-scored $\Delta F/F$ to the onset of each trial of a behaviour, averaging across all trials for each animal and then averaging across animals. For each recording session, the responses during a behaviour period were calculated as the AUC per second during all trials of a behaviour.

In vitro electrophysiological recording

For in vitro whole-cell patch-clamp recordings, mice were anaesthetized with isoflurane, and the brains were removed and submerged in ice-cold cutting solution containing 110 mM choline chloride, 25 mM $NaHCO_3$, 2.5 mM KCl, 7 mM $MgCl_2$, 0.5 mM $CaCl_2$, 1.25 mM NaH_2PO_4, 25 mM glucose, 11.6 mM ascorbic acid and 3.1 mM pyruvic acid. Then, 275 μm coronal sections were cut using the Leica VT1200s vibratome and incubated in artificial cerebral spinal fluid containing 125 mM NaCl, 2.5 mM KCl, 1.25 mM NaH_2PO_4, 25 mM $NaHCO_3$, 1 mM $MgCl_2$, 2 mM $CaCl_2$ and 11 mM glucoses at 34 °C for 30 min and then at room temperature until use. The intracellular solution for current-clamp recording contained 145 mM K-gluconate, 2 mM $MgCl_2$, 2 mM Na_2ATP, 10 mM HEPES, 0.2 mM EGTA (286 mOsm, pH 7.2). The intracellular solution for the voltage clamp recording contained 135 mM $CsMeSO_3$, 10 mM HEPES, 1 mM EGTA, 3.3 mM QX-314 (chloride salt), 4 mM Mg-ATP, 0.3 mM Na-GTP and 8 mM sodium phosphocreatine (pH 7.3 adjusted with CsOH). The signals were acquired using the MultiClamp 700B amplifier and digitized at 20 kHz using DigiData1550B (Molecular Devices). The recorded electrophysiological data were analysed using Clampfit (Molecular Devices) and MATLAB (Mathworks).

To determine the intrinsic excitability of $MPOA^{ESR1}$ and $BNSTpr^{ESR1}$ cells, we performed current-clamp recordings and injected 30 current steps ranging from −20 pA to 270 pA in 10 pA increments into the recorded cell. The total number of spikes during each 500-ms-long current step was then used to construct the F–I curve.

We performed voltage-clamp recordings of $BNSTpr^{ESR1}$ and $MPOA^{ESR1}$ neurons. To record oEPSCs and oIPSCs, the cell membrane potential was held at −70 mV and 0 mV, respectively. To activate ChR2-expressing axons, we delivered brief pulses of full-field illumination (0.5 ms, 0.1 Hz, 10 times) onto the recorded cell with a blue LED light (pE-300 white; CoolLED). We then applied TTX (1 μM), 4-AP (100 mM), gabazine (2 μM), and strychnine (5 μM) through the bath solution sequentially, each for 10–20 min. Data acquisition started at least 5 min after each drug application.

To validate the ArchT-mediated terminal inactivation, we performed voltage-clamp recordings of $BNSTpr^{ESR1}$ (for $MPOA^{ESR1}$–BNSTpr projection) and $MPOA^{ESR1}$ (for $BNSTpr^{ESR1}$–MPOA projection) cells with a holding potential of 0 mV. We activated ChR2-expressing axons by delivering brief blue light pulses (0.5 ms duration, 20 repeats) of full field LED illumination (pE-300 white; CoolLED) and simultaneously delivered 5 mW yellow light (Shanghai dream laser) or not to the recorded cell through a 400 μm optic fibre placed right above the recording site.

Immunohistochemistry and imaging analysis

Mice were perfused with 1 × PBS followed with 4% PFA. Brains were dissected, post-fixed in 4% PFA overnight at 4 °C, rinsed with 1 × PBS and dehydrated in 30% sucrose for 12–16 h. Then, 30 μm sections were cut

using the Leica CM1950 cryostat. For brain-wide FOS staining, every one in three brain slices of the whole brain was collected. For ESR1 staining, every one in three brain slices of BNSTpr region was collected. Then, free-floating brain slices were rinsed three times with PBS (10 min) and once with PBST (0.1% Triton X-100 in PBS, 30 min) at room temperature, followed by 1 h of blocking in 10% normal donkey serum at room temperature. The primary antibody (guinea pig anti-FOS, 1:500 dilution, Synaptic Systems, 226005; rabbit anti-ESR1, 1:3,000 dilution, Millipore, 06-935, 3243424) was diluted in PBST with 3% normal donkey serum and incubated overnight (12–16 h) at 4 °C. Brain slices were then washed three times with PBST (10 min) and incubated with the secondary antibody (secondary antibody for FOS staining, Cy3-goat anti-guinea pig, 1:500 dilution, Jackson ImmunoResearch, 706-165-148; secondary antibody for ESR1 staining, Cy5- donkey anti-rabbit, 1:500 dilution, Jackson ImmunoResearch, 711-175-152) for 2 h at room temperature. Brain slices were then washed three times with PBST (10 min), rinsed with 1× PBS and mounted onto superfrost slides (Thermo Fisher Scientific, 12-550-15), dried for 10 min at room temperature and coverslipped in 50% glycerol containing DAPI (Invitrogen, 00-4959-52). Images were acquired using a slide scanner (Olympus, VS120) or a confocal microscope (Zeiss LSM 700 microscope). Brain regions were identified on the basis of the Allen Mouse Brain Atlas, and cells were counted manually using ImageJ.

We counted FOS-expressing cells in each brain region (note that every third brain section was collected for staining) and divided it by the region's size as the density of FOS^+ cells. To compare $FOS^+Tracer^+$ and $FOS^-Tracer^+$ cells among different behaviour groups, we counted the total $FOS^+Tracer^+$ and $FOS^-Tracer^+$ cells in each region across all animals and compared the cell numbers across groups. For the relative projection density of $BNSTpr^{ESR1}$ and $MPOA^{ESR1}$ cells, the average fluorescence intensity in each region containing presynaptic GFP^+ puncta was first quantified as the average pixel value of the region and then normalized to the average fluorescence intensity of the start region.

Statistics

No statistical methods were used to predetermine sample sizes, but our sample sizes are similar to those reported in previous publications[18,43,51–53]. All experiments were conducted using 2 to 4 cohorts of animals. The results were reproducible across cohorts and combined for the final analysis. All statistical analyses were performed using MATLAB and Prism software. Fisher's exact test was used on unpaired nominal data from two groups. McNemar's test was used on paired nominal data from two groups. All statistical analyses were two-tailed. If distributions passed Kolmogorov–Smirnov or Shapiro–Wilk tests for normality, parametric tests—including paired *t*-test and one-way ANOVA followed by a multiple-comparisons test corrected using the two-stage linear step-up procedure of Benjamini, Krieger and Yekutieli—were used to determine whether there was any statistically significant difference between the means of two or more groups. For comparing among multiple groups and multiple treatment conditions, two-way repeated-measures ANOVA followed by multiple-comparisons tests corrected using the two-stage linear step-up procedure of Benjamini, Krieger and Yekutieli were used. If distributions did not pass normality tests, Mann–Whitney U-tests, Wilcoxon matched-pairs signed-rank tests and mixed-effects analysis followed by multiple-comparisons test corrected using the two-stage linear step-up procedure of Benjamini, Krieger and Yekutieli were used. For all statistical tests, significance was measured against an alpha value of 0.05. Detailed statistical results are provided as Source Data.

Reporting summary

Further information on research design is available in the Nature Portfolio Reporting Summary linked to this article.

Data availability

Fibre photometry recording data, behaviour annotations and raw representative histology images are available at Zenodo (https://doi.org/10.5281/zenodo.7772552). Behaviour videos and additional histology images are available from the corresponding author on reasonable request. Source data are provided with this paper.

Code availability

MATLAB code used in this study is available at Zenodo (https://doi.org/10.5281/zenodo.7772552).

50. Mathis, A. et al. DeepLabCut: markerless pose estimation of user-defined body parts with deep learning. *Nat. Neurosci.* **21**, 1281–1289 (2018).
51. Yin, L. et al. $VMHvll^{Cckar}$ cells dynamically control female sexual behaviors over the reproductive cycle. *Neuron* **110**, 3000–3017 (2022).
52. Wong, L. C. et al. Effective modulation of male aggression through lateral septum to medial hypothalamus projection. *Curr. Biol.* **26**, 593–604 (2016).
53. Falkner, A. L. et al. Hierarchical representations of aggression in a hypothalamic-midbrain circuit. *Neuron* **106**, 637–648 (2020).

Acknowledgements We thank all of the members of the Lin laboratory for discussions; and Y. Jiang for assisting with genotyping. This research was supported by NIH grants R01MH101377, R01MH124927 and U19NS107616 (to D.L.), R01HD092596 (to D.L. and R.M.S.), and R37HD083217 (to R.M.S.); the Mathers Foundation, and the Vulnerable Brain Project (to D.L.); and the Levy Leon Postdoctoral Fellowship (to L.M.).

Author contributions D.L. and L.M. conceived the project, designed experiments, analysed data and wrote the paper. D.L. supervised the project. L.M. performed most of the experiments and prepared figures. R.Y. and L.Y. performed slice recording experiments and prepared related figures. R.M.S. provided critical feedback on the experiments.

Competing interests The authors declare no competing interests.

Additional information

Supplementary information The online version contains supplementary material available at https://doi.org/10.1038/s41586-023-06147-9.

Correspondence and requests for materials should be addressed to Long Mei or Dayu Lin.

Peer review information *Nature* thanks Minmin Luo and the other, anonymous, reviewer(s) for their contribution to the peer review of this work. Peer reviewer reports are available.

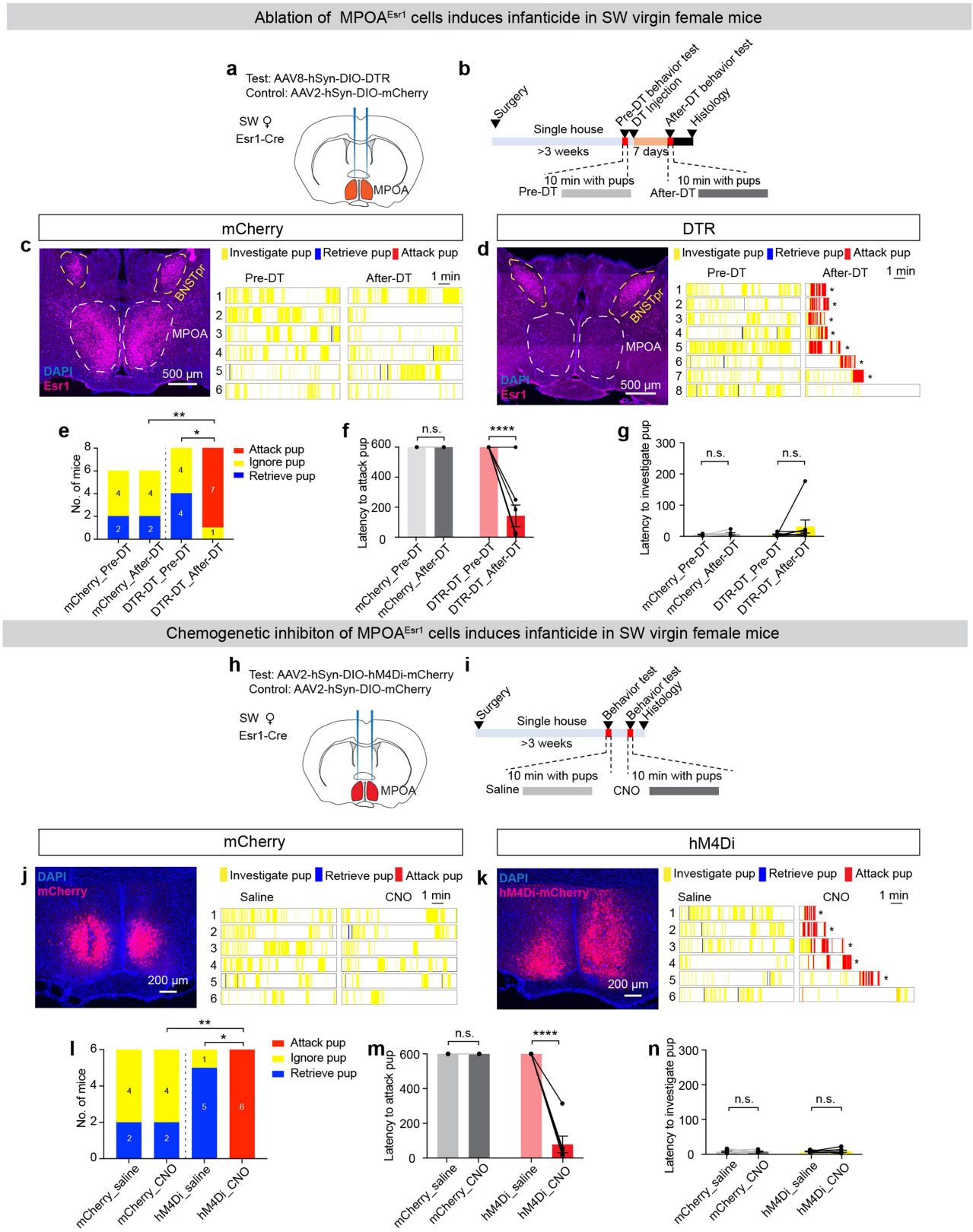

Extended Data Fig. 1 | See next page for caption.

Extended Data Fig. 1 | Ablation or chemogenetic inhibition of MPOA^{Esr1} cells induces infanticide in SW virgin female mice. (**a**) Experimental design to ablate MPOA^{Esr1} cells. (**b**) Experimental timeline. (**c**,**d**) Left showing representative histology images of Esr1 staining (magenta) in MPOA and BNSTpr after DT injection in a mCherry female of 6 mice(**c**) and a DTR female of 8 mice (**d**). Right showing raster plots of pup-directed behaviours in mCherry (**c**) and DTR females (**d**) before and after i.p. injection of DT. *Remove wounded pups and stop recording. (**e**) Number of mCherry and DTR virgin females that attack, ignore or retrieve pups before and after DT injection. Fisher's exact test for comparing behaviours (attack vs. no attack) between groups before or after DT injection. McNemar's test for comparing behaviours (attack vs. no attack) between pre-DT and after-DT within a group. * $p < 0.05$. ** $p < 0.01$. (**f**,**g**) Latency to attack pup (**f**) and investigate pup (**g**) before and after DT injection in mCherry and DTR females. If the behaviour of interest is not observed during the entire session, the latency is 600 s. Error bars: ± SEM. Mixed-effects analysis followed with multiple comparisons test. **** $p < 0.0001$. n = 6 mice for mCherry group, n = 8 mice for DTR group. (**h**) Experimental design to chemogenetically inhibit MPOA^{Esr1} cells. (**i**) Experimental timeline. (**j**,**k**) Left showing representative histology images of mCherry (**j**) and hM4Di-mCherry (**k**) expression of 6 mice each group in MPOA. Right showing raster plots of pup-directed behaviours in mCherry (**j**) and hM4Di females (**k**) after i.p. injection of saline or CNO. *Remove wounded pups and stop recording. (**l**) Number of mCherry and hM4Di virgin females that attack, ignore or retrieve pups after saline or CNO injection. Fisher's exact test for comparing behaviours (attack vs. no attack) between groups after saline or CNO injection. McNemar's test for comparing behaviours (attack vs. no attack) between saline and CNO injections within a group. * $p < 0.05$. ** $p < 0.01$. (**m**,**n**) Latency to attack pup (**m**) and investigate pup (**n**) after saline or CNO injection in mCherry and hM4Di females. Error bars: ± SEM. Mixed-effects analysis (**m**) and Two-way RM ANOVA (**n**) followed with multiple comparisons test. **** $p < 0.0001$. n = 6 mice for each group. Brain illustrations in (**a**) and (**h**) are produced based on reference atlas from https://atlas.brain-map.org/.See Source Data Extended Data Fig. 1 for detailed values and statistics.

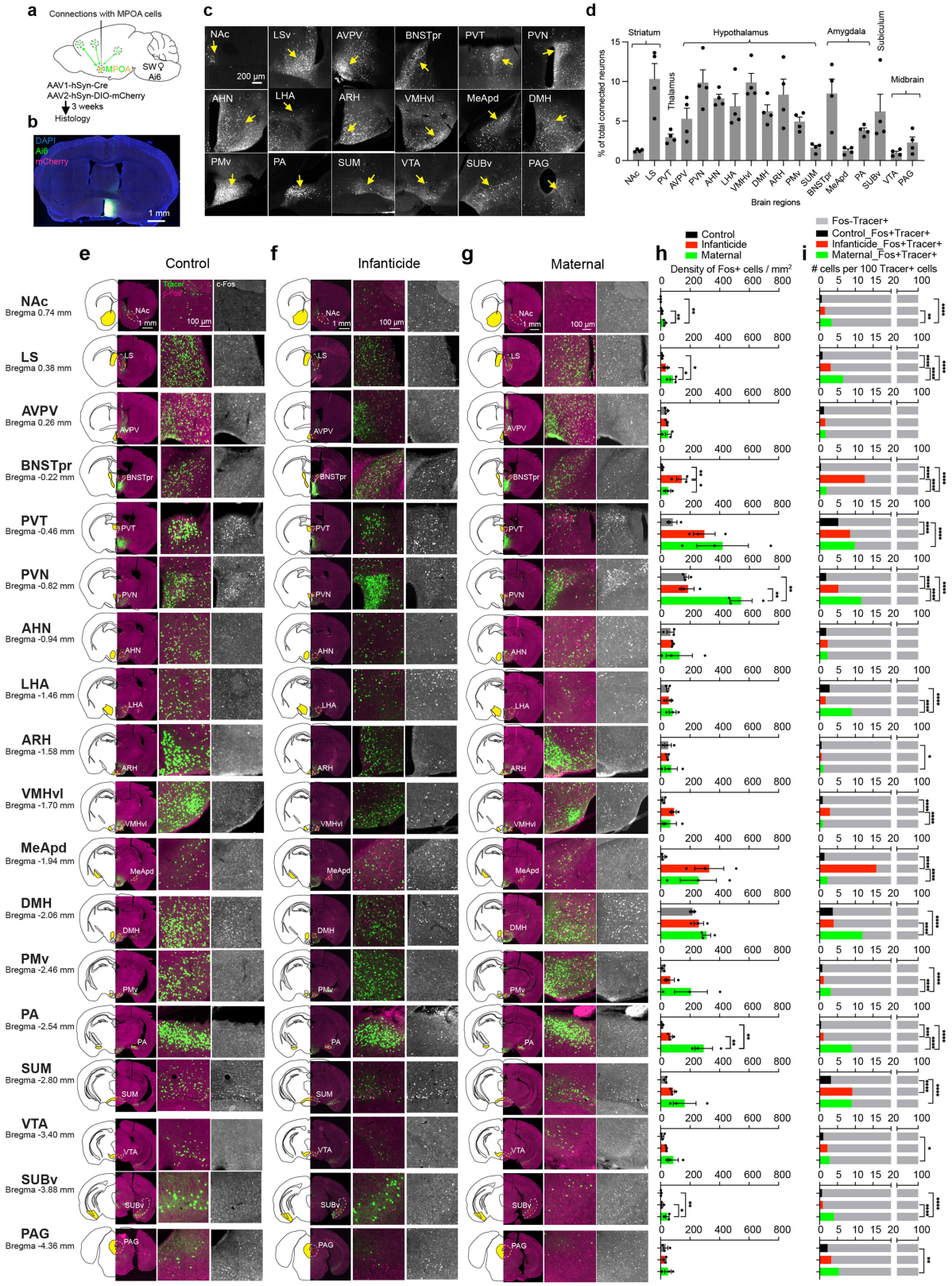

Extended Data Fig. 2 | See next page for caption.

Extended Data Fig. 2 | MPOA-connecting cells across brain regions and their overlap with Infanticide and maternal care induced c-Fos. (**a**) Experimental design to trace MPOA-connecting cells throughout the brain using Ai6 female mice and high titre (> 1×10^{13} vg/mL) AAV1-hSyn-Cre. (**b** and **c**) Images from a representative animal of 4 mice showing the primary injection site in the MPOA (**b**) and MPOA-connecting cells in various brain areas (**c**). Scale bars: 1 mm (**b**) and 200 µm (**c**). (**d**) Distribution of MPOA-connecting neurons in various brain regions. All regions containing over 1% of total labelled cells are shown. n = 4. Error bars: SEM. (**e**–**g**) Representative images of 3 mice each group of 18 regions showing baseline (**e**), infanticide-induced (**f**), and maternal behaviour-induced (**g**) c-Fos and zsGreen expression in Ai6 female mice injected with AAV1-hSyn-Cre into the MPOA. Baseline c-Fos are from females left undisturbed in the home cage. Brain illustrationsare produced based on reference atlas from https://atlas.brain-map.org/. (**h**) The density of c-Fos expressing cells in each MPOA-connecting brain region in control, infanticidal and maternal female mice. n = 3 mice for each group. One-way ANOVA followed with multiple comparisons test. *p < 0.05, **p < 0.01, Error bars: ±SEM. (**i**) The total number of Fos+Tracer+ and Fos-Trace+ cells per 100 Tracer+ cells in each MPOA-connecting brain region in control, infanticidal and maternal female mice. n = 3 mice for each group. Fisher's exact test is based on unnormalized total numbers of Fos+Tracer+ and Fos-Trace+ cells of each group. *p < 0.05, **p < 0.01, ***p < 0.001, ****p < 0.0001. See Source Data Extended Data Fig. 2 for detailed values and statistics.

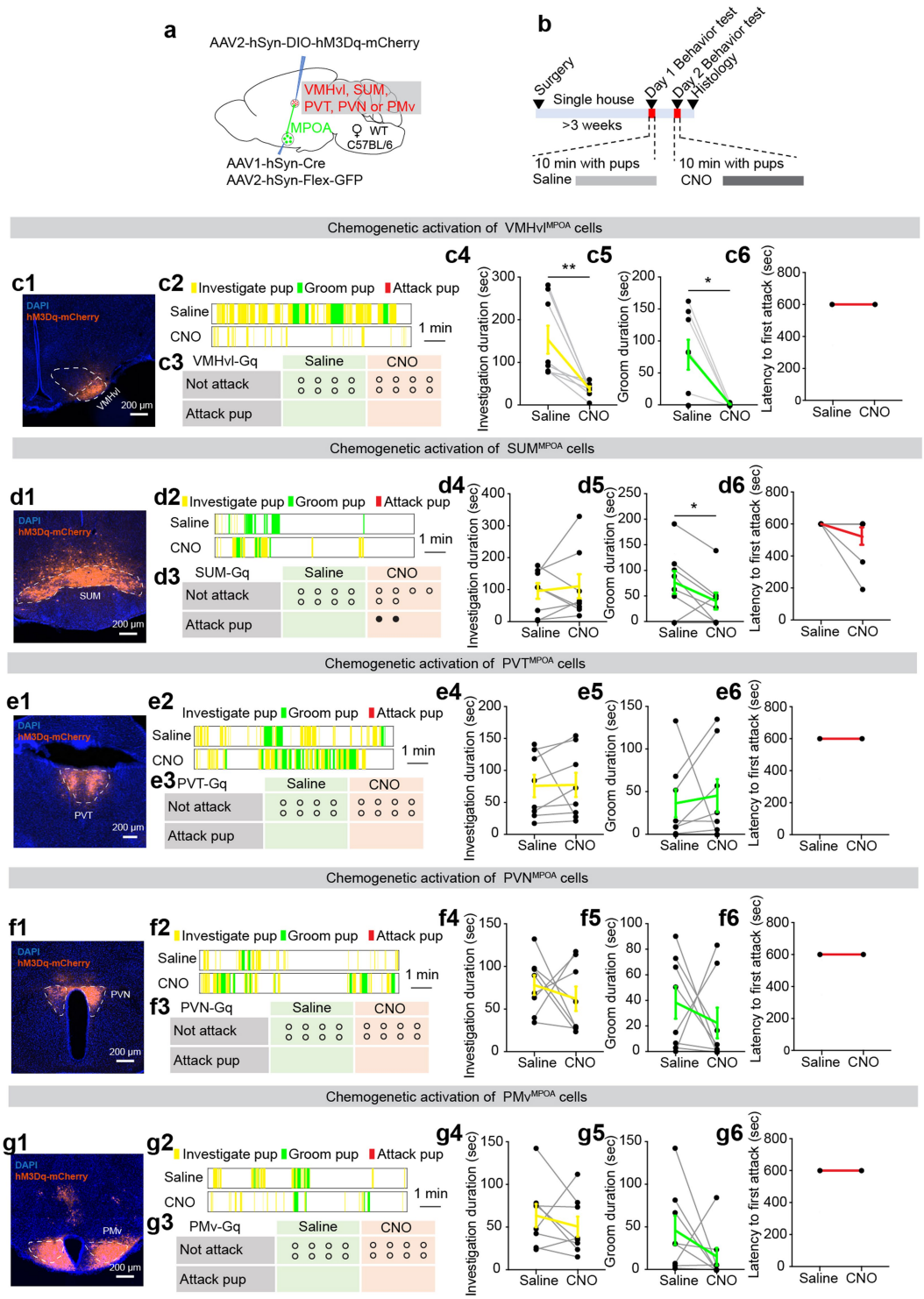

Extended Data Fig. 3 | See next page for caption.

Extended Data Fig. 3 | Pup-directed behaviours after chemogenetic activation of MPOA-connecting cells in the VMHvl, SUM, PVT, PVN, or PMv in female mice. (**a**) Experimental design to chemogenetically activate various MPOA-connecting regions. (**b**) Experimental timeline. **(c1**, **d1**, **e1**, **f1**, **g1**) Representative histology images of 8 mice showing hM3Dq-mCherry expression in the VMHvl (**c1**), SUM (**d1**), PVT (**e1**), PVN (**f1**), and PMv (**g1**) after injecting AAV1-Syn-Cre in MPOA and AAV2-hSyn-DIO-hM3Dq-mCherry into each of the regions. Scale bars: 200 µm. **(c2**, **d2**, **e2**, **f2**, **g2**) Representative raster plots showing pup-directed behaviours after saline or CNO injection into animals expressing hM3Dq-mCherry in MPOA-connecting cells in the VMHvl (**c2**), SUM (**d2**), PVT (**e2**), PVN (**f2**), and PMv (**g2**). Each raster lasts 10 min. **(c3**, **d3**, **e3**, **f3**, **g3**) Pup-directed attack after saline or CNO injection in female mice that express hM3Dq-mCherry in MPOA-connecting cells in the VMHvl (**c3**), SUM (**d3**), PVT (**e3**), PVN (**f3**), and PMv (**g3**). Each circle represents one mouse. n = 8 for each group. **(c4**, **d4**, **e4**, **f4**, **g4**) Duration of pup investigation between saline- and CNO-injected days in female mice that express hM3Dq-mCherry in MPOA-connecting cells in the VMHvl (**c4**), SUM (**d4**), PVT (**e4**), PVN (**f4**), and PMv (**g4**). Each grey line represents one animal. The coloured line represents the group average. Error bars: ± SEM. Wilcoxon matched-pairs signed rank test (**c4**) or Two-tailed Paired t test (**d4**, **e4**, **f4**, **g4**). $^{**}p < 0.01$. n = 8 for each group. **(c5**, **d5**, **e5**, **f5**, **g5**) Duration of pup grooming between saline- and CNO-injected days in female mice that express hM3Dq-mCherry in MPOA-connecting cells in the VMHvl (**c5**), SUM (**d5**), PVT (**e5**), PVN (**f5**), and PMv (**g5**). Figure conventions as in **c4**-**g4**. (**c6**, **d6**, **e6**, **f6**, **g6**) Latency to first pup attack between saline- and CNO-injected days in female mice that express hM3Dq-mCherry in MPOA-connecting cells in the VMHvl (**c6**), SUM (**d6**), PVT (**e6**), PVN (**f6**), and PMv (**g6**). Figure conventions as in **c4**-**g4**. See Source Data Extended Data Fig. 3 for detailed values and statistics.

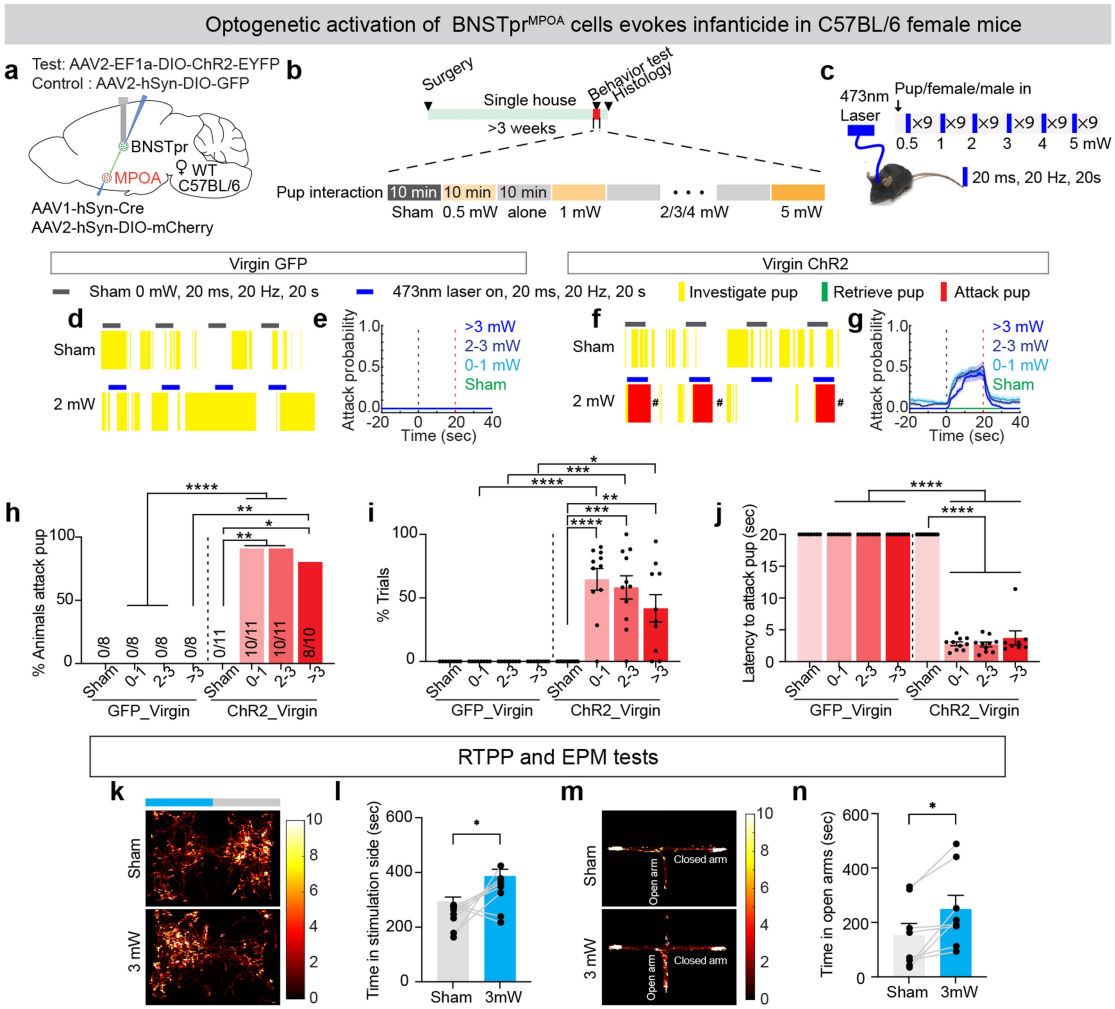

Extended Data Fig. 4 | Optogenetic activation of BNSTpr^{MPOA} neurons elicits infanticide, induces real-time place preference, and reduces anxiety in female mice. (**a**) Experimental design to optogenetically activate BNSTpr^{MPOA} cells. (**b**) Experimental timeline. (**c**) Light delivery protocol. (**d** and **f**) Representative raster plots showing pup-directed behaviours during sham and 2 mW light stimulation in virgin female mice expressing GFP (**d**) or ChR2-EYFP (**f**) in BNSTpr^{MPOA} cells. # Remove wounded pup(s) and introduce a new pup. (**e** and **g**) PETH of attack pup probability in virgin female mice expressing GFP (**e**) and virgin female mice expressing ChR2-EYFP (**g**) in BNSTpr^{MPOA} cells following sham or light stimulation. Only trials with female-pup contact are included for analysis. Left black dash line: Light on. Right red dash line: light off. (**h**) Percentage of animals that attacked pups in GFP and ChR2 group. Fisher's exact test for comparison between GFP and ChR2 group. McNemar's test for comparison between sham and different laser intensity within ChR2 group. *p < 0.05, **p < 0.01, ****p < 0.0001. n = 8 mice for GFP control, n = 11 mice for ChR2 virgin group (sham, 0-1, 2-3), n = 10 mice for ChR2 virgin group (>3). (**i**) Percentage of trials showing pup attack. Each dot represents one mouse. Error bars: ± SEM. Mixed-effects analysis followed with multiple comparisons test. *p < 0.05, **p < 0.01, ***p < 0.001, ****p < 0.0001. n = 8 mice for GFP control, n = 11 mice for ChR2 virgin group (sham, 0-1, 2-3), n = 10 mice for ChR2 virgin group (>3). (**j**) Averaged latency to attack pup upon encountering the pup following sham or light stimulation. Error bars: ± SEM. Mixed-effects analysis followed with multiple comparisons test. ****p < 0.0001. n = 8 mice for GFP control, n = 11 mice for ChR2 virgin group (sham, 0-1, 2-3), n = 10 mice for ChR2 virgin group (>3). (**k**-**l**) Representative tracking results during the RTPP test (**k**) and the time spent in sham or 3 mW stimulation chamber (**l**). n = 8 mice. Paired t test. *p < 0.05. Error bars: SEM. (**m**-**n**) Representative tracking results during an EPM test (**m**) and the time spent in open arms (**n**) with sham or 3 mW laser stimulation. n = 8 mice. Paired t test. *p < 0.05. Error bars: SEM. See Source Data Extended Data Fig. 4 for detailed values and statistics.

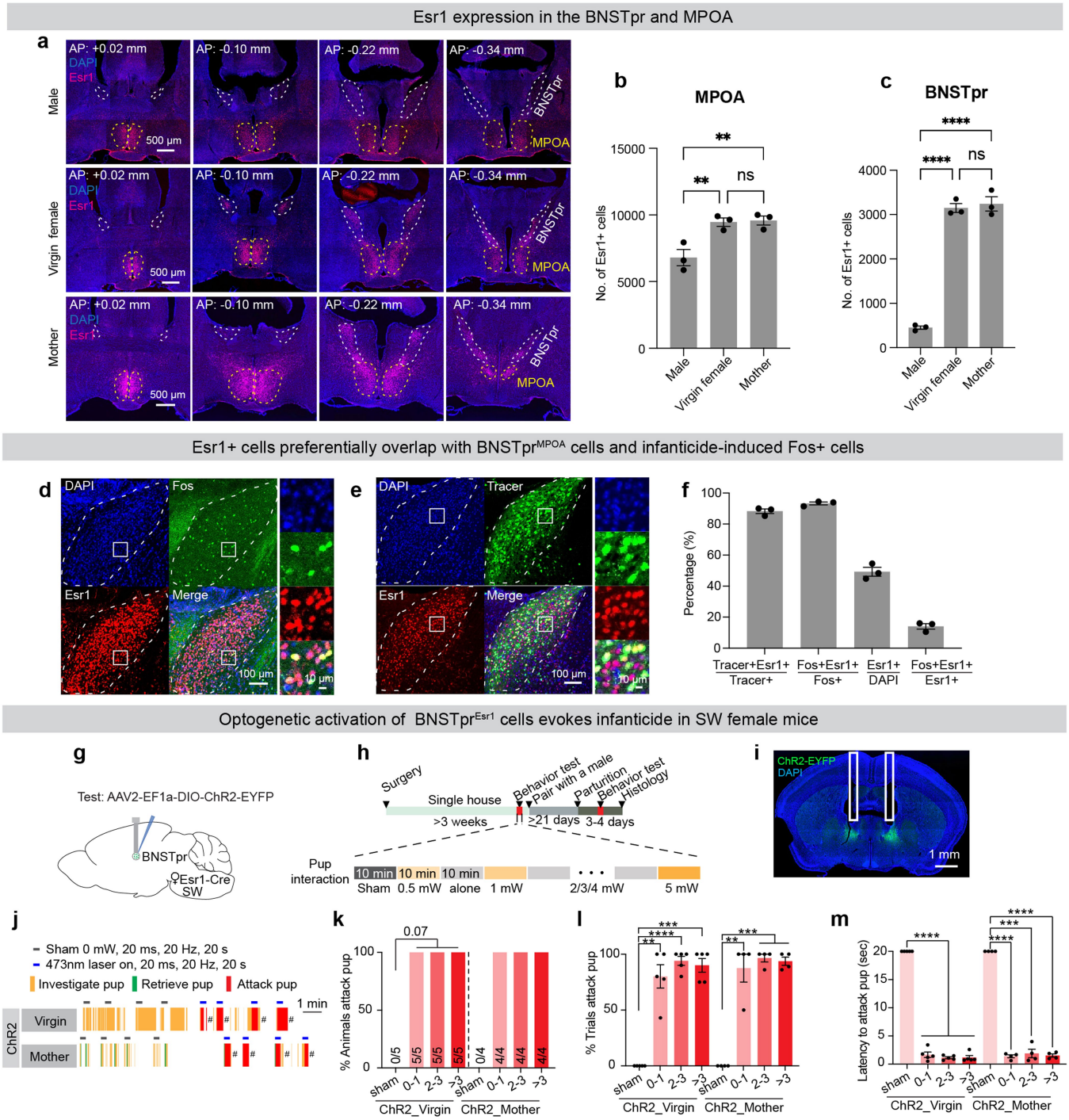

Extended Data Fig. 5 | See next page for caption.

Extended Data Fig. 5 | Additional characterization of BNSTpr Esr1 cells and their activation-induced infanticide in SW female mice. (**a**) Representative coronal sections of 3 mice each group showing Esr1 immunostaining in MPOA and BNSTpr in a male (top), a virgin female (middle) and a mother (bottom). Scale bars: 500 µm. (**b**, **c**) Number of Esr1 positive cells in the MPOA (**b**) and BNSTpr (**c**) in male, virgin female, and mother mice. n = 3 mice for each group. One-way ANOVA followed with multiple comparisons test. **p < 0.01, ****p < 0.0001. Error bars: ± SEM. (**d**) Representative images of 3 mice showing overlap between Esr1 (red) and infanticide-induced c-Fos (green) in the BNSTpr. Right shows the enlarged view of the boxed area. Scale bars: 100 µm (left) and 10 µm (right). (**e**) Representative images of 3 mice showing the overlap between Esr1 (red) and zsGreen (green) in the BNSTpr in an Ai6 animals injected with AAV1-hSyn-Cre at the MPOA. Right shows the enlarged view of the boxed area. Scale bars: 100 µm (left) and 10 µm (right). (**f**) Quantification of overlap between MPOA-connected cells, Esr1 and the infanticide-induced c-Fos in the BNSTpr. n = 3 mice for each group, Error bars: ± SEM. (**g**) Experimental design to optogenetically activate BNSTpr^{Esr1} cells in non-infanticidal SW virgin females. (**h**) Experimental timeline. (**i**) Representative image of 4 mice showing ChR2 expression (green) in the BNSTpr and fibre tracks (while boxes). Scale bar: 1 mm. (**j**) Representative raster plots showing pup-directed behaviours during sham and 2 mW light stimulation in a non-infanticidal SW virgin female (top) and a mother (bottom) expressing ChR2-EYFP in BNSTpr^{Esr1} cells. # Replace a wounded pup. (**k**) Percentage of animals that attack pups. n = 5 mice for ChR2 virgin group, n = 4 mice for ChR2 mother group. McNemar's test for comparison between sham and different laser intensity within each ChR2 group. (**l**) Percentage of trials showing pup attack. Each dot represents one mouse. Mean ± SEM. Mixed-effects analysis followed with multiple comparisons test. **p < 0.01, ***p < 0.001, ****p < 0.0001. n = 5 mice for ChR2 virgin group, n = 4 mice for ChR2 mother group. (**m**) Average latency to attack pup upon encountering the pup following sham or light stimulation. Error bars: ± SEM. Mixed-effects analysis followed with multiple comparisons test. ***p < 0.001, ****p < 0.0001. n = 5 mice for ChR2 virgin group, n = 4 mice for ChR2 mother group. See Source Data Extended Data Fig. 5 for detailed values and statistics.

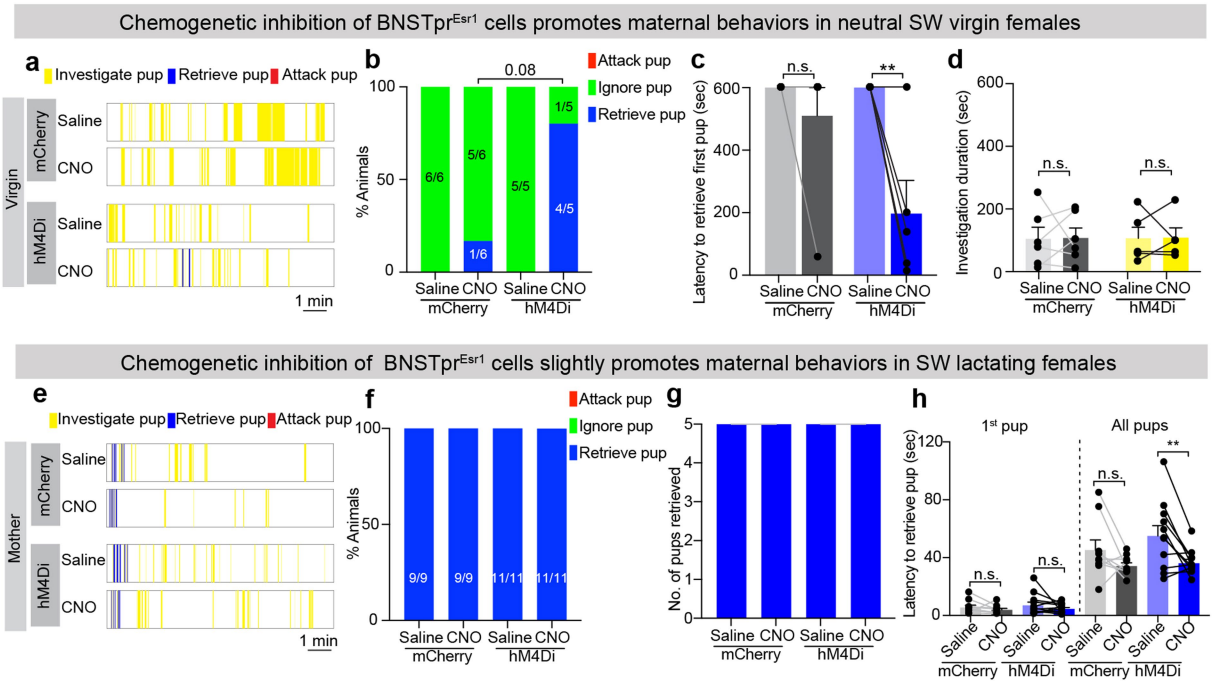

Extended Data Fig. 6 | Chemogenetic inhibition of BNSTpr^{Esr1} neurons promotes maternal behaviour in non-hostile virgin females and mothers. (**a**) Representative raster plots showing pup-directed behaviours in non-hostile non-maternal mCherry and hM4Di virgin females after saline or CNO injection. (**b**) Percentage of mCherry and hM4Di virgin females that ignore, retrieve or attack pups after saline or CNO injection. Fisher's exact test between mCherry and hM4Di group. (**c**,**d**) Latency to retrieve pup (**c**) and pup investigation duration (**d**) after saline or CNO injection in non-hostile non-maternal virgin mCherry and hM4Di females. Error bars: ± SEM. n = 6 mice for mCherry group; n = 5 mice for hM4Di group. Mixed-effects analysis followed with multiple comparisons test. **p < 0.01. (**e**) Representative raster plots showing various pup-directed behaviours in lactating mCherry and hM4Di females after saline or CNO injection. (**f**) All mCherry and hM4Di lactating females retrieved pups after saline or CNO injection. (**g**) All 5 pups were retrieved in the 10-min testing period in mCherry and hM4Di lactating females after either saline or CNO injection. n = 9 mice for mCherry group; n = 11 mice for hM4Di group. (**h**) Latency to retrieve the first pup and all five pups in mCherry and hM4Di lactating females after saline or CNO injection. Error bars: SEM. n = 9 mice for mCherry group; n = 11 mice for hM4Di group. Mixed-effects analysis followed with multiple comparisons test. **p < 0.01. See Source Data Extended Data Fig. 6 for detailed values and statistics.

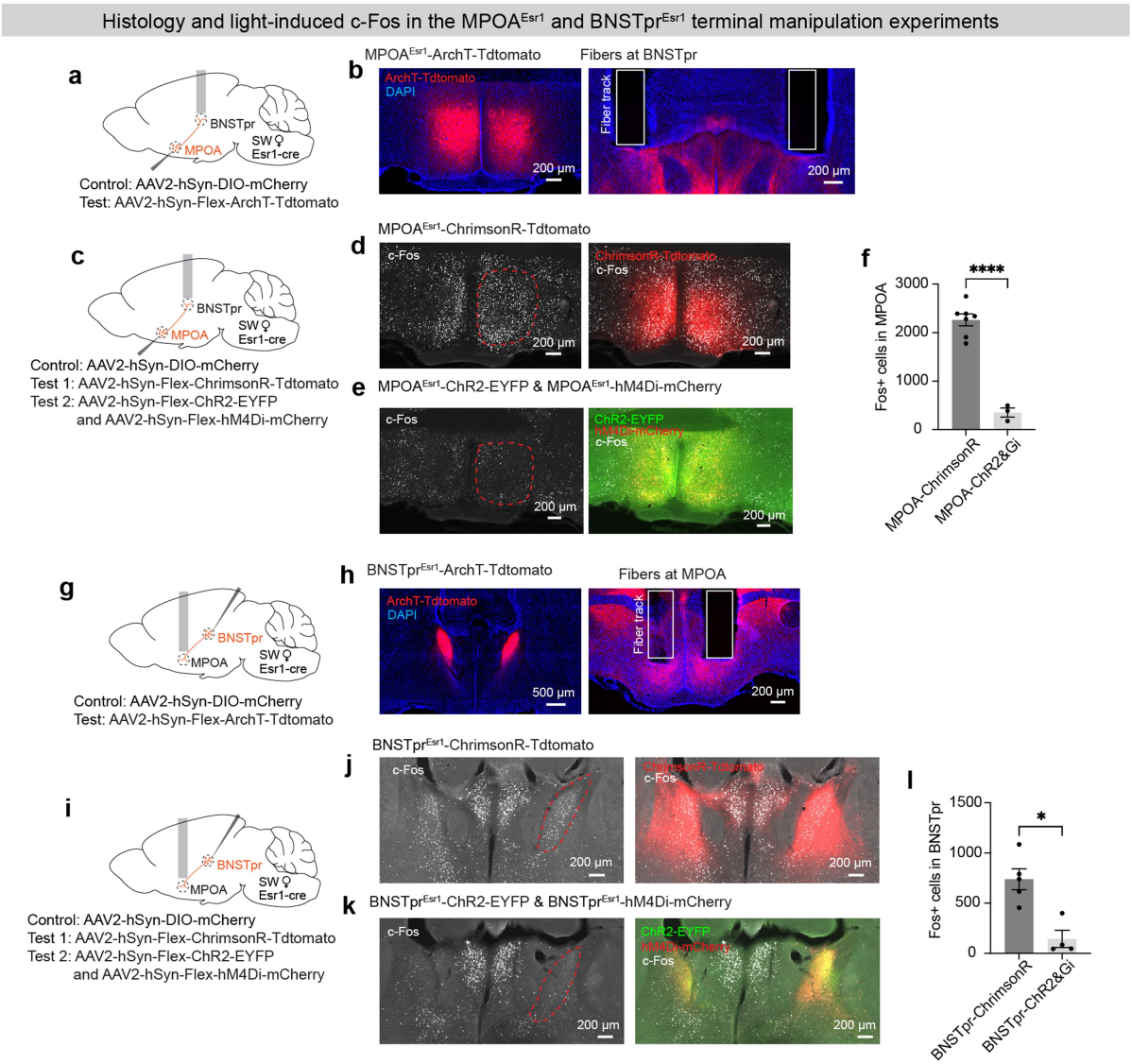

Extended Data Fig. 7 | Histology and light-induced c-Fos in the MPOA^{Esr1} and BNSTpr^{Esr1} terminal manipulation experiments. (**a**) Experimental design to optogenetically inactivate MPOA^{Esr1} inputs to BNSTpr. (**b**) Representative histology of 6 mice showing ArchT expression (red) in the MPOA (left), and ArchT expression terminals and optic fibre tracks in the BNSTpr (right). (**c**) Experimental design to optogenetically activate MPOA^{Esr1} inputs to the BNSTpr. (**d**) Representative histology of 7 mice showing ChrimsonR (red) and c-Fos (white) in the MPOA after delivering 5 mW pulsed yellow light to the right side of the BNSTpr for 10 min. (**e**) Representative histology of 3 mice showing ChR2 (green), hM4Di (red), and c-Fos (white) in the MPOA after delivering 10 min 5 mW pulsed blue light to the right side of the BNSTpr 30 min after CNO injection. (**f**) Number of c-Fos+ cells in the right MPOA in ChrimsonR and ChR2+Gi group. Error bars: ± SEM. Unpaired t test, ****$p < 0.0001$. n = 7 mice for ChrimsonR group, n = 3 for ChR2+Gi group. (**g**) Experimental design to optogenetically inactivate BNSTpr^{Esr1} inputs to MPOA. (**h**) Representative histology of 6 mice showing ArchT (red) in the BNSTpr (left), and ArchT expressing axons and optic fibre tracks in the MPOA (right). (**i**) Experimental design to optogenetically activate BNSTpr^{Esr1} inputs to MPOA. (**j**) Representative histology of 5 mice showing ChrimsonR (red) and c-Fos (white) in the BNSTpr after delivering 5 mW pulsed yellow light to the right side of the MPOA for 10 min. (**k**) Representative histology of 4 mice showing ChR2 (green), hM4Di (red) and c-Fos (white) in BNSTpr after delivering 10 min 5 mW pulsed blue light to the right MPOA 30 min after CNO injection. (**l**) Number of c-Fos+ cells in the right BNSTpr in ChrimsonR and ChR2+Gi group. Error bars: ± SEM. Mann Whitney test, *$p < 0.05$. n = 5 mice for ChrimsonR group, n = 4 for ChR2+Gi group. See Source Data Extended Data Fig. 7 for detailed values and statistics.

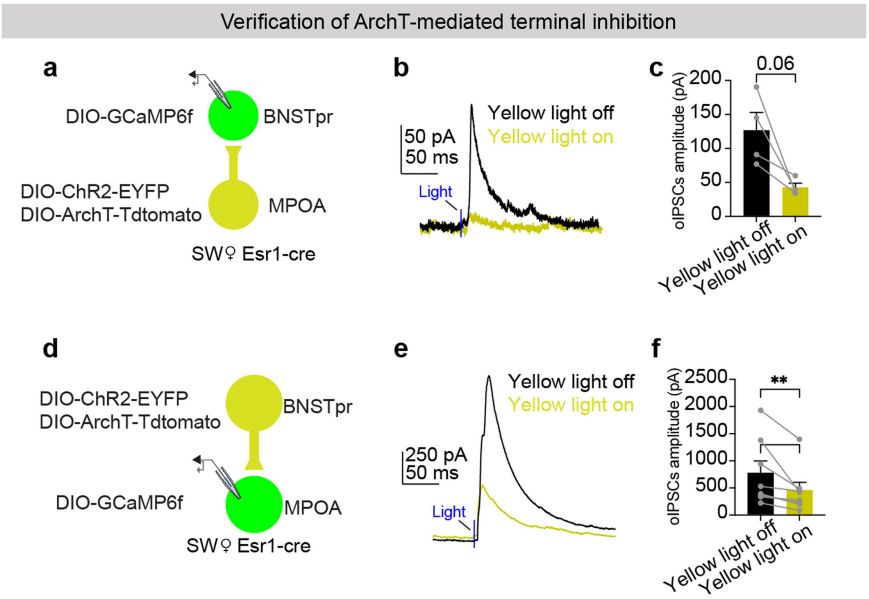

Extended Data Fig. 8 | Verification of ArchT-mediated terminal inhibition. (**a** and **d**) Experimental design to examine the efficacy of ArchT-mediated inhibition of MPOA^{Esr1} → BNSTpr^{Esr1} (**a**) and BNSTpr^{Esr1} → MPOA^{Esr1} (**d**) projections. (**b** and **e**) Representative blue light pulse evoked IPSCs from BNSTpr^{Esr1} (**b**) and MPOA^{Esr1}cells (**e**) with (yellow) and without (black) simultaneous 5 mW yellow light delivery. (**c** and **f**) The amplitude of oIPSCs of BNSTpr^{Esr1} (**c**) and MPOA^{Esr1} cells (**f**) with and without 5 mW yellow light delivery. Error bars: ± SEM. Paired t-test (**c**) and Wilcoxon matched-pairs signed rank test (**f**), **p < 0.01. n = 4 BNSTpr^{Esr1} cells, n = 8 MPOA^{Esr1} cells. See Source Data Extended Data Fig. 8 for detailed values and statistics.

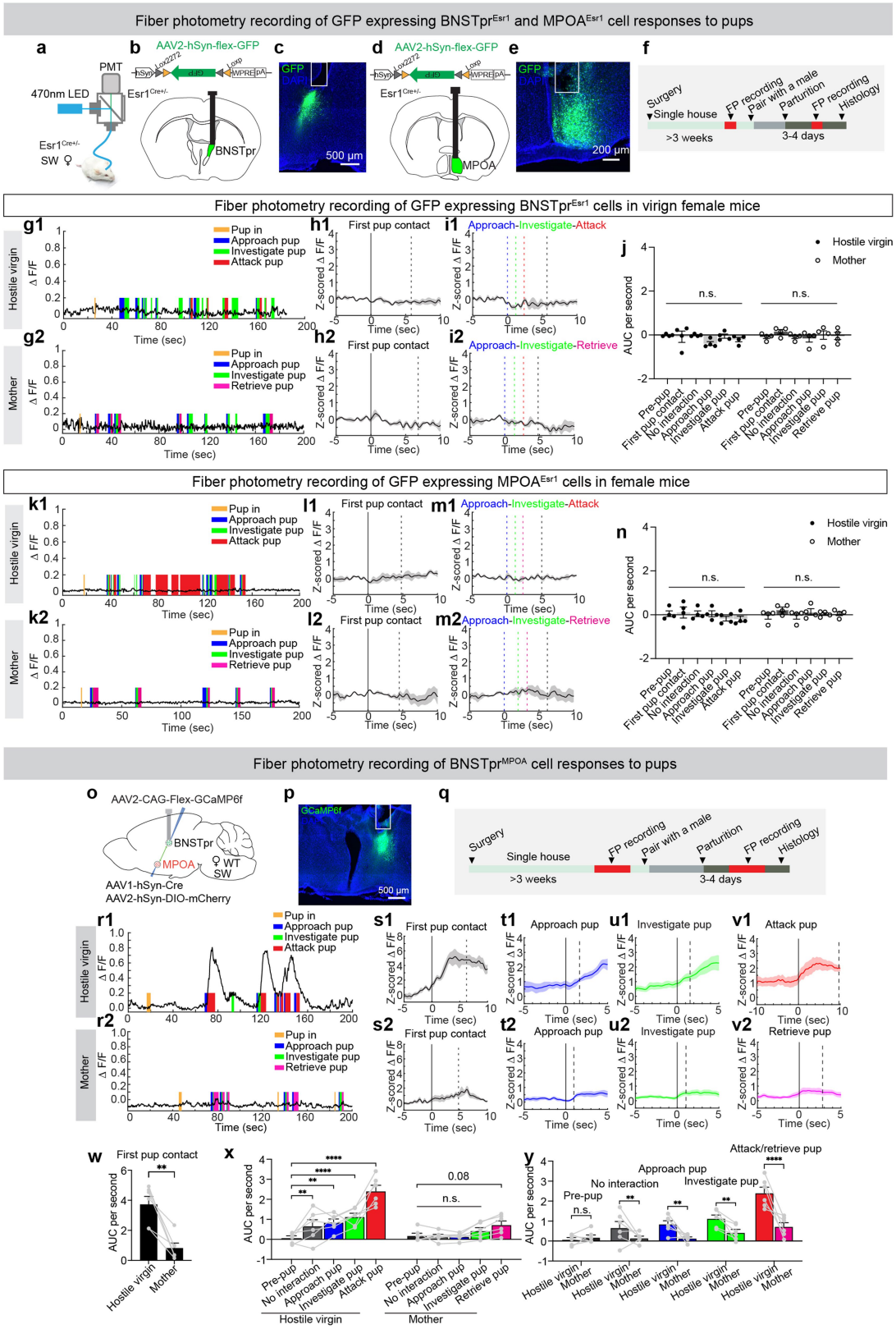

Extended Data Fig. 9 | See next page for caption.

Extended Data Fig. 9 | Fibre photometry recording of GFP-expressing BNSTpr^{Esr1} and MPOA^{Esr1} cells and GCaMP6f-expressing BNSTpr^{MPOA} cells during pup interaction. (**a**) Fibre photometry setup. (**b** and **d**) Viral construct and targeted brain regions. Brain illustrations are produced based on reference atlas from https://atlas.brain-map.org/. (**c** and **e**) Representative histological images of 4 mice showing GFP (green) expression and fibre tracks (white box) in BNSTpr (**c**) and MPOA (**e**). (**f**) Experimental timeline. (**g**,**k**) Representative GFP recording (ΔF/F) traces of BNSTpr^{Esr1} (**g**) and MPOA^{Esr1} (**k**) cells during pup interaction in a hostile SW virgin female (**g1**, **k1**) and a mother (**g2**, **k2**). Colour shades indicate various behaviours. (**h**,**l**) PETHs of GFP signal (Z-scored ΔF/F) of BNSTpr^{Esr1} (**h**) and MPOA^{Esr1} (**l**) cells aligned to the first pup contact in hostile virgin females (**h1**, **l1**), and mothers (**h2**, **l2**). n = 4 mice. Solid lines indicate the onset on first pup contact; dashed black lines indicate the mean duration of first pup contact. Shades: ± SEM. (**i**,**m**) PETHs of GFP signal (Z-scored ΔF/F) of BNSTpr^{Esr1} (**i**) and MPOA^{Esr1} (**m**) cells aligned to the onset of pup approach in hostile virgin females (**i1**, **m1**), and mothers (**i2**, **m2**). n = 4 mice for each group. Blue dashed lines indicate the onset of pup approach; green dashed lines indicate the mean latency to pup investigation; the red and black dashed lines in **i1** and **m1** indicate the mean latency to attack and stop attacking pups, respectively; the magenta and black dashed lines in **i2** and **m2** indicate the mean latency to retrieve and stop retrieving pups, respectively. Shades: ± SEM. (**j**,**n**) Mean AUC of Z-scored ΔF/F signal of BNSTpr^{Esr1} (**j**) and MPOA^{Esr1} (**n**) cells during various pup-directed behaviours in hostile virgin females and mothers. Two-way RM ANOVA (**j**) and Mixed-effects analysis (**n**) followed with multiple comparisons test. n = 4 mice for each group. Error bars: ± SEM. (**o**) Experimental design. (**p**) A representative histological image of 9 mice showing GCaMP6f (green) expression and the fibre track in BNSTpr (white lines). (**q**) Experimental timeline. (**r**) Representative GCaMP6f recording (ΔF/F) traces of BNSTpr^{MPOA} cells during pup interaction in a hostile SW virgin female (**r1**) and a mother (**r2**). Colour shades indicate various behaviours. (**s**–**v**) PETHs of GCaMP6f signal (Z-scored ΔF/F) of BNSTpr^{MPOA} cells aligned to the onset of various behaviours in hostile virgin females (**s1**-**v1**), and mothers (**s2**-**v2**). n = 6 mice. Solid lines indicate the onset on each behaviour; dashed black lines indicate the end of each behaviour. Shades: ± SEM. (**w**) Mean AUC of Z-scored ΔF/F signal of BNSTpr^{MPOA} cells during the first pup contact. Paired t-test. $^{**}p < 0.01$. Error bars: SEM. n = 6 mice. (**x**,**y**) Mean AUC of Z-scored ΔF/F signal of BNSTpr^{MPOA} cells during pre-pup period and various pup-directed behaviours in hostile virgin females and mothers. Two-way RM ANOVA followed with multiple comparisons test. $^{**}p < 0.01$, $^{****}p < 0.0001$, mean ± SEM. n = 6 mice. See Source Data Extended Data Fig. 9 for detailed values and statistics.

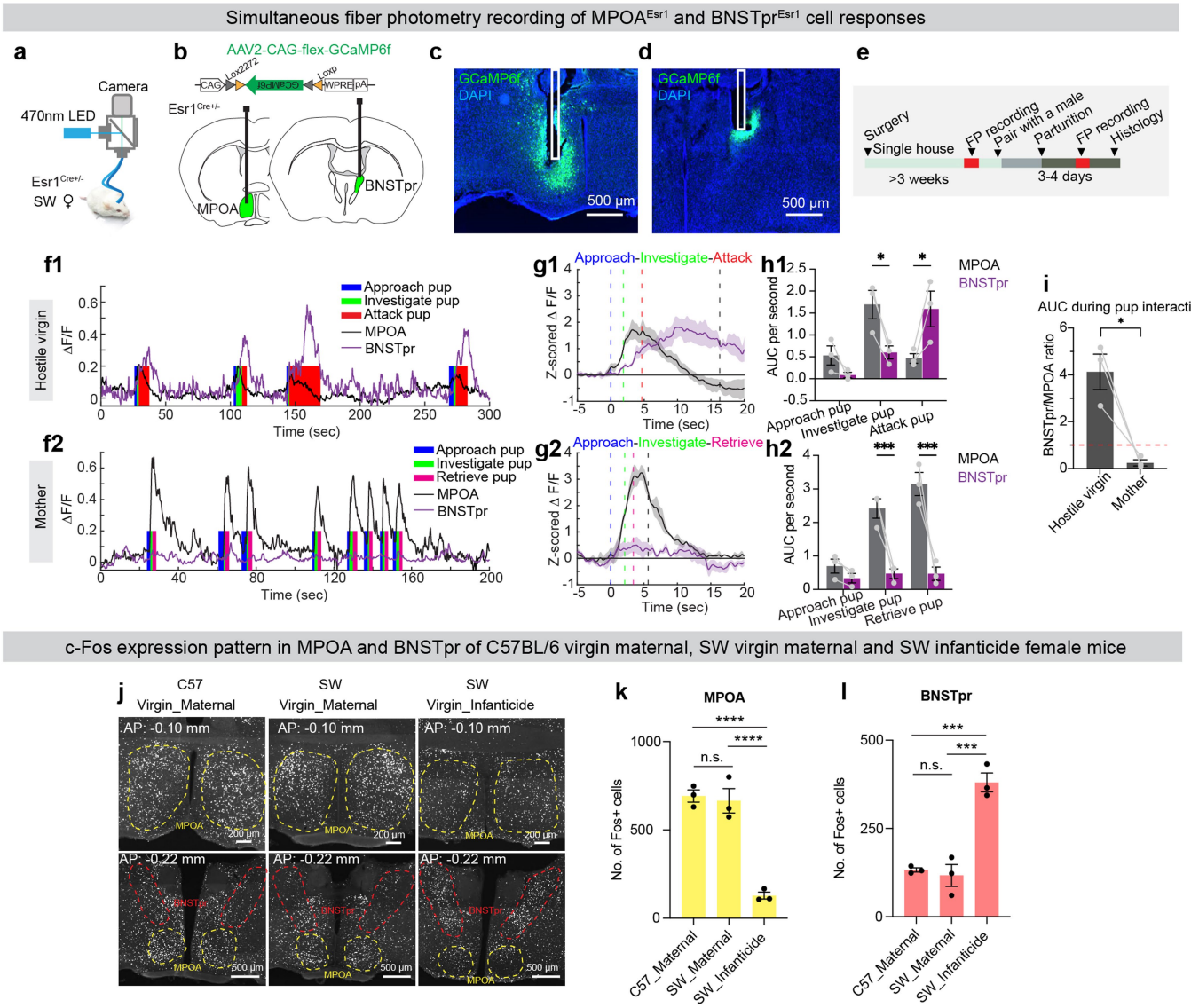

Extended Data Fig. 10 | Simultaneous recording of MPOA^{Esr1} and BNSTpr^{Esr1} cells and comparing infanticide and maternal behaviour-induced c-Fos between strains. (**a**) Fibre photometry setup. (**b**) Viral construct and targeted brain regions. Brain illustrations are produced based on reference atlas from https://atlas.brain-map.org/. (**c**,**d**) Representative histological images of 3 mice showing GCaMP6f (green) expression and fibre tracks (white boxes) in MPOA (**c**) and BNSTpr (**d**). (**e**) Experimental timeline. (**f**) Representative GCaMP6f recording (ΔF/F) traces of MPOA^{Esr1} (black) and BNSTpr^{Esr1} (purple) cells during pup interaction in a hostile SW virgin female (**f1**) and a mother (**f2**). Colour shades indicate various behaviours. (**g**) PETHs of GCaMP6f signal (Z-score ΔF/F) of MPOA^{Esr1} (black) and BNSTpr^{Esr1} (purple) cells aligned to the onset of pup approach in hostile virgin females (**g1**), and mothers (**g2**). n = 3 mice for each group. Blue dashed lines indicate the onset of pup approach; green dashed lines indicate the mean latency to pup investigation; the red and black dashed lines in **g1** indicate the mean latency to attack and stop attacking pups, respectively; the magenta and black dashed lines in **g2** indicate the mean latency to retrieve and stop retrieving pups, respectively. Shades: ± SEM. (**h**) Mean AUC of Z-scored ΔF/F signal of MPOA^{Esr1} (black) and BNSTpr^{Esr1} (purple) cells during pup approach, investigation, attack, and retrieval in hostile virgin females (**h1**) and mothers (**h2**). Two-way RM ANOVA (**h1**) and Mixed-effects analysis (**h2**) followed with multiple comparisons test. n = 3 mice for each group, *p < 0.05, ***p < 0.001, mean ± SEM. (**i**) BNSTpr^{Esr1} and MPOA^{Esr1} response ratio in hostile virgin females and mothers during pup interaction period. The red dashed line indicates 1. n = 3 mice for each group, Paired *t-test*. *p < 0.05, mean ± SEM. (**j**) Representative histological images of 3 mice in each group showing c-Fos expression in MPOA and BNSTpr of a C57BL/6 virgin maternal female (left), a SW virgin maternal female (middle), and a SW infanticidal female (right). (**k**, **l**) Number of c-Fos+ cells in MPOA (**k**) and BNSTpr (**l**) in C57BL/6 virgin maternal, SW virgin maternal and SW infanticidal female mice. n = 3 for each group, ***p < 0.001, ****p < 0.0001. Error bars: ± SEM. One-way ANOVA followed with multiple comparisons test. See Source Data Extended Data Fig. 10 for detailed values and statistics.

nature portfolio

Corresponding author(s): Long Mei, Dayu Lin

Last updated by author(s): Mar 26, 2023

Reporting Summary

Nature Portfolio wishes to improve the reproducibility of the work that we publish. This form provides structure for consistency and transparency in reporting. For further information on Nature Portfolio policies, see our Editorial Policies and the Editorial Policy Checklist.

Statistics

For all statistical analyses, confirm that the following items are present in the figure legend, table legend, main text, or Methods section.

n/a	Confirmed
☐	☒ The exact sample size (*n*) for each experimental group/condition, given as a discrete number and unit of measurement
☐	☒ A statement on whether measurements were taken from distinct samples or whether the same sample was measured repeatedly
☐	☒ The statistical test(s) used AND whether they are one- or two-sided *Only common tests should be described solely by name; describe more complex techniques in the Methods section.*
☐	☒ A description of all covariates tested
☐	☒ A description of any assumptions or corrections, such as tests of normality and adjustment for multiple comparisons
☐	☒ A full description of the statistical parameters including central tendency (e.g. means) or other basic estimates (e.g. regression coefficient) AND variation (e.g. standard deviation) or associated estimates of uncertainty (e.g. confidence intervals)
☐	☒ For null hypothesis testing, the test statistic (e.g. *F*, *t*, *r*) with confidence intervals, effect sizes, degrees of freedom and *P* value noted *Give P values as exact values whenever suitable.*
☒	☐ For Bayesian analysis, information on the choice of priors and Markov chain Monte Carlo settings
☒	☐ For hierarchical and complex designs, identification of the appropriate level for tests and full reporting of outcomes
☒	☐ Estimates of effect sizes (e.g. Cohen's *d*, Pearson's *r*), indicating how they were calculated

Our web collection on statistics for biologists contains articles on many of the points above.

Software and code

Policy information about availability of computer code

Data collection	Fiber photometry data was using a custom TDT program as described previously (Fang, Y.Y., et al. 2018, Neuron; Yamaguchi, T., et al. 20220, Nat Neurosci). Animal behaviors were recorded from both top and side using two synchronized cameras (Edmund, stock #89533) controlled by StreamPix (Version 5; NORPIX, https://www.norpix.com/products/streampix/streampix.php) at 25 frames/sec.
Data analysis	All statistical analysis were performed using MATLAB (R2018a), Prism (v9, GraphPad) and Fiji (2.11.0) software. Behaviors were analyzed manually frame-by-frame using a custom software written in MATLAB (https://pdollar.github.io/toolbox/). MATALB code used in this study can be downloaded from 10.5281/zenodo.7772552.

For manuscripts utilizing custom algorithms or software that are central to the research but not yet described in published literature, software must be made available to editors and reviewers. We strongly encourage code deposition in a community repository (e.g. GitHub). See the Nature Portfolio guidelines for submitting code & software for further information.

Data

Policy information about availability of data

All manuscripts must include a data availability statement. This statement should provide the following information, where applicable:

- Accession codes, unique identifiers, or web links for publicly available datasets
- A description of any restrictions on data availability
- For clinical datasets or third party data, please ensure that the statement adheres to our policy

Source data are provided with this paper. Behavioral analysis code can be found (https://pdollar.github.io/toolbox/). Raw values associated with each figure panel can be found in the source data files. Fiber photometry recording data, behavior annotations and raw representative histology images can be downloaded from 10.5281/zenodo.7772552. Behavior videos and additional histology images are available from the corresponding author upon reasonable request.

Human research participants

Policy information about studies involving human research participants and Sex and Gender in Research.

Reporting on sex and gender	*Use the terms sex (biological attribute) and gender (shaped by social and cultural circumstances) carefully in order to avoid confusing both terms. Indicate if findings apply to only one sex or gender; describe whether sex and gender were considered in study design whether sex and/or gender was determined based on self-reporting or assigned and methods used. Provide in the source data disaggregated sex and gender data where this information has been collected, and consent has been obtained for sharing of individual-level data; provide overall numbers in this Reporting Summary. Please state if this information has not been collected. Report sex- and gender-based analyses where performed, justify reasons for lack of sex- and gender-based analysis.*
Population characteristics	*Describe the covariate-relevant population characteristics of the human research participants (e.g. age, genotypic information, past and current diagnosis and treatment categories). If you filled out the behavioural & social sciences study design questions and have nothing to add here, write "See above."*
Recruitment	*Describe how participants were recruited. Outline any potential self-selection bias or other biases that may be present and how these are likely to impact results.*
Ethics oversight	*Identify the organization(s) that approved the study protocol.*

Note that full information on the approval of the study protocol must also be provided in the manuscript.

Field-specific reporting

Please select the one below that is the best fit for your research. If you are not sure, read the appropriate sections before making your selection.

☒ Life sciences ☐ Behavioural & social sciences ☐ Ecological, evolutionary & environmental sciences

For a reference copy of the document with all sections, see nature.com/documents/nr-reporting-summary-flat.pdf

Life sciences study design

All studies must disclose on these points even when the disclosure is negative.

Sample size	Sample sizes were not predetermined using statistical methods. Sample sizes were chosen to reliably measure experimental effects while minimizing the number of animals used in accordance with ethical guidelines. Our sample sizes are similar to previous studies (e.g. Fang, Y.Y., et al. 2018, Neuron; Yamaguchi, T., et al. 20220, Nat Neurosci), and are deemed appropriate based on the size and statistical significance of the effects and consistency across animals.
Data exclusions	For Fiber photometry recording, mice that do not went through the whole pregnant to become mothers were not used. All the mice excluded in this study has clearly reported in the method
Replication	Fiber photometry recording, immunohistochemistry, pharmacogenetic activation and inactivation, optogenetic neural activation and in vitro electrophysiological recordings were replicated in multiple animals (see statistic summary in each source data table for exact numbers of animals for each experiment).
Randomization	In Figure 1b, 1c. animals were choose base on the behavior (infanticide nor not) needed. In figure 1d-q, animals were randomly assigned to experimental or control group. In figure 2d-l, non-infanticide mice were randomly assigned to experimental or control group. In figure 2p-s, infanticide mice were randomly assigned to experimental or control group. In figure 3, mice were randomly assigned. In figure 4a-4e, 4p-4t, non-infanticide mice were randomly assigned to experimental or control group. In figure 4f-4o, infanticide mice were randomly assigned to experimental or control group.

In figure 5, infanticide mice were randomly assigned to start with BNSTpr or MPOA recording in virgin state, then the same mice were recording in maternal virgin state and when they become mothers.
In figure 5a-5e. mice were randomly assigned to MPOA or BNSTpr recording base on their behavior and reproductive states needed with the experiments design.
In figure f-i, mice were distributed base on the genetic background needed by the experiments design.
In Extended data figure 1. non-infanticide mice were randomly assigned to experimental or control group.
In Extended data figure 2a-d. mice were randomly assigned.
In Extended data figure 2e-i. mice were assigned based on their behavior towards pup which is needed by the experiments design.
In Extended data figure 3, non-infanticide mice were randomly assigned to experimental or control group.
In Extended data figure 4, non-infanticide mice were randomly assigned to experimental or control group.
In Extended data figure 5a-c, mice were assigned based on sex and reproductive stage which is needed by the experiments design.
In Extended data figure 5d-f, mice were randomly assigned
In Extended data figure 5g-m, non-infanticide mice were first record during virgin state, then paired with male, after they becomes mother, they were test again, so we can have with animal comparison.
In Extended data figure 6. non-infanticide mice were randomly assigned to experimental or control group.
In Extended data figure 8. mice were randomly assigned to either projection direction.
In Extended data figure 9a-m. infanticide mice were randomly assigned to start recording in MPOA or BNSTpr.
In Extended data figure 9o-y, infanticide mice were first record in virgin state, then paired with male, after they becomes mother, they were recorded again.
In Extended data figure 10a-i, infanticide mice were first record in virgin state, then paired with male, after they becomes mother, they were recorded again.
In Extended data figure 10j-l, mice were assigned based on the genetic background and behavior towards pup which is needed by the experiments design.
In supplementary note 1_Figure1d-k, animals were the same mice used main figure 5h-o, so we can have with animal comparison
In supplementary note 1_Figure1o-v, animals were the same mice used Extended data figure 9r-v, so we can have with animal comparison
In supplementary note 1_Figure2, mice were randomly assigned to experimental or control group.
In supplementary note 1_Figure3, mice were randomly assigned to experimental or control group.
In supplementary note 1_Figure4, mice were randomly assigned to experimental or control group.

Blinding

Experimenters were not blind to group allocation during data acquisition or analysis. We make sure that control and experiments group were test in the same condition, and data were analyzed with the same criteria.

Reporting for specific materials, systems and methods

We require information from authors about some types of materials, experimental systems and methods used in many studies. Here, indicate whether each material, system or method listed is relevant to your study. If you are not sure if a list item applies to your research, read the appropriate section before selecting a response.

Materials & experimental systems

n/a	Involved in the study
☐	☒ Antibodies
☒	☐ Eukaryotic cell lines
☒	☐ Palaeontology and archaeology
☐	☒ Animals and other organisms
☒	☐ Clinical data
☒	☐ Dual use research of concern

Methods

n/a	Involved in the study
☒	☐ ChIP-seq
☒	☐ Flow cytometry
☒	☐ MRI-based neuroimaging

Antibodies

Antibodies used

1. Guinea pig anti-Fos (Synaptic Systems, Cat. # 226005)
2. Rabbit anti-Esr1 (Millipore, Cat. # 06-935)
3. Goat anti-Guinea pig Cyanine Cy™3 (Jackson ImmunoResearch, Cat. # 706-165-148)
4. Donkey anti-rabbit Cyanine Cy™5 (Jackson ImmunoResearch, Cat. # 711-175-152)

Validation

1. Guinea pig anti-Fos (Synaptic Systems, Cat. # 226005). Validated by the company and other groups. (https://www.sysy.com/product/226005#list)
2. Rabbit anti-Esr1 (Millipore, Cat. # 06-935). Validated by the company and other groups. (https://www.emdmillipore.com/US/en/product/Anti-Estrogen-Receptor-Antibody,MM_NF-06-935#anchor_REF)
3. Goat anti-Guinea pig Cyanine Cy™3 (Jackson ImmunoResearch, Cat. # 706-165-148). Validated by the company and other groups. (https://www.citeab.com/antibodies/2036154-706-165-148-cy3-affinipure-donkey-anti-guinea-pig-ig?utm_campaign=Widget+All+Citations&utm_medium=Widget&utm_source=Jackson+Immunoresearch&utm_term=Jackson+ImmunoResearch)
4. Donkey anti-rabbit Cyanine Cy™5 (Jackson ImmunoResearch, Cat. # 711-175-152). Validated by the company and other groups. (https://www.citeab.com/antibodies/2036198-711-175-152-cy5-affinipure-donkey-anti-rabbit-igg-h?utm_campaign=Widget+All+Citations&utm_medium=Widget&utm_source=Jackson+Immunoresearch&utm_term=Jackson+ImmunoResearch)

Animals and other research organisms

Policy information about studies involving animals; ARRIVE guidelines recommended for reporting animal research, and Sex and Gender in Research

Laboratory animals	Esr1-2A-Cre mice were provided initially by D.J. Anderson lab (Caltech) and are currently available from Jackson Laboratory (stock no. 017911). Esr1-2A-Cre mice with SW background were backcrossed with SW wildtype mice for at least five generations. All experimental Esr1-2A-Cre mice are heterozygous. Ai6 mice were purchased from the Jackson Laboratory (stock no. 007906) and were backcrossed to either SW or C57 for at least five generations. Wildtype SW mice were purchased from Taconic. Wildtype C57BL/6 and Balb/c mice were purchased from Charles River, P1-P5 pups used for behavioral experiments were bred in-house. Mice were housed in 12 h light-dark cycle (10 p.m. – 10 a.m. light), with food and water available ad libitum. Temperature and humidity: ~22°C with ~45% humidity. All mice were group housed until adulthood. After surgery, mice were single housed unless they were paired with a male, and after they became pregnant, they were single housed again until having a litter.
Wild animals	No wild animals were used in this study.
Reporting on sex	All animals sex were clearly reported.
Field-collected samples	No field-collected samples were used in this study.
Ethics oversight	All animal experiments were performed in accordance with NIH guidelines and approved by the New York University medical school Institutional Animal Care and Use Committee (IACUC).

Note that full information on the approval of the study protocol must also be provided in the manuscript.